Appendix N. Pc Calculation Approaches – UPDATE 3/20/24

N.1 Introduction

This appendix discusses the selection of the Probability of Collision (Pc) as the risk assessment parameter to use for conjunction assessment requirements compliance. While this parameter is widely used in the conjunction assessment industry, issues related to its calculation exist that merit extended discussion. The most frequently used analytical techniques to calculate the Pc are well established and computationally efficient but include assumptions that restrict their use and make the calculations vulnerable to error for a small fraction of conjunctions. Numerical techniques also exist, such as Monte Carlo Pc estimation. Predictably, these make fewer assumptions and are more widely applicable, but they are much more computationally demanding. There are also issues related to the regularization and interpretation of the input data to the Pc calculation, some of which are resolved by techniques that are now becoming standard practices. In calculating Pc estimates, it is necessary to examine and prepare the input datasets carefully and then to choose the calculation approach that is appropriate to the situation. The purpose of this appendix is to amplify the Pc calculation-related recommendations by providing an extended technical explanation of the data preparation and Pc calculation issues so that implementers and users of these calculations can proceed with a better understanding of the different options and resultant fidelities of Pc calculation.

To accomplish this goal, this appendix will address the following technical areas:

- A step-by-step description of the conjunction plane two-dimensional Pc calculation, which is the most established and widely used analytical Pc computation technique, and its enabling simplifications and assumptions;
- Examination and repair/expansion of input data to the calculation, focusing mostly on the orbital state covariance matrices for the two objects in conjunction;
- Discussion of the use of Monte Carlo techniques, which is the numerical method used for high-fidelity Pc computation;
- A test to determine whether an analytical or numerical technique should be used for a particular conjunction;
- Approaches to choosing for the Pc calculation the hard-body radius, which gives a statement of the combined sizes of the primary and secondary objects; and
- Discussion of alternative analytic Pc calculation methods, specifically the two- and three-dimensional “Nc” (as opposed to “Pc”) estimation methods that address conjunctions affected by curvilinear trajectories and non-Gaussian distribution effects.
- Discussion of correcting Pc estimates for covariance cross correlation effects, which affects some conjunctions involving high-drag satellites.

N.2 Conjunction Plane Analytic Pc Calculation

The conjunction plane method of Pc calculation, which is by far the most widely used approach in the conjunction assessment industry, was developed for the Space Shuttle Program and first described in the literature in 1992 (Foster and Estes). There have been a number of important treatments since that time — e.g., Akella and Alfriend (2000), Patera (2001), Alfano (2005a), Chan (2008), Garcia-Pelayo (2016), and Elrod (2019) — but all rely on the same basic methodology: applying reasonable assumptions to enable analytical approximations. While the particulars vary, these approaches all share the same concept of calculating the Pc estimate by integrating over a two-dimensional region on a conjunction encounter plane.

Conjunction plane Pc analysis begins with the states and covariances for the primary and secondary objects' orbital states at TCA. An important set of questions should be addressed concerning whether these data, especially the covariances, are truly representative of the expected states and uncertainties at TCA or whether the propagation process has distorted them. These questions will be addressed in a subsequent section, once a more focused context for them has been established through the present discussion of the general procedure.

The first step is to recognize that Pc calculations depend on the relative positions and uncertainties of the two objects, so moving to a framework that views the problem this way is helpful. Subtraction of the two objects' positions produces a relative position vector, the magnitude of which is the miss distance between the two objects (at TCA). Similarly, because interest is in the relative rather than absolute position uncertainty, it is possible to combine the two objects' covariances to form a joint (relative) covariance and allocate that, if desired, to one "end" of the relative position vector (by convention the end for the secondary object), as shown in Figure N-1. There are, of course, questions regarding whether the two covariances are independent and can be combined by simple addition; this question is addressed in a later section, but it is typically acceptable to presume independence and combine the covariances in this manner.

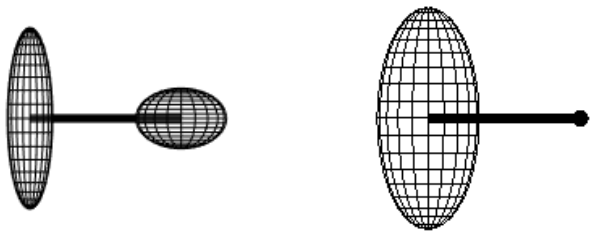

Figure N-1 Relative Positions and Uncertainties of Two Objects

The second step relates to modeling the combined sizes of the primary and secondary objects. The general approach is to place a circumscribing sphere about the primary (whose size is well known by the O/O because it is their satellite) and then do the same thing for the secondary but often via an estimation technique as the secondary is usually a debris object for which there is no definitive size information. If these two spheres approach and begin to overlap one another at any point during the encounter, then a potential collision has been identified. Again, keeping in mind that a relative framework is useful here, the two objects' size spheres can be combined into one super-sphere (also called the "collision sphere") and placed at one end, by convention the

primary object end, of the relative miss vector, as shown in Figure N-2. If the miss vector should shrink to be smaller than the radius of the collision sphere (also called the hard-body radius), that would be the equivalent of the two original spheres encroaching on each other at TCA.

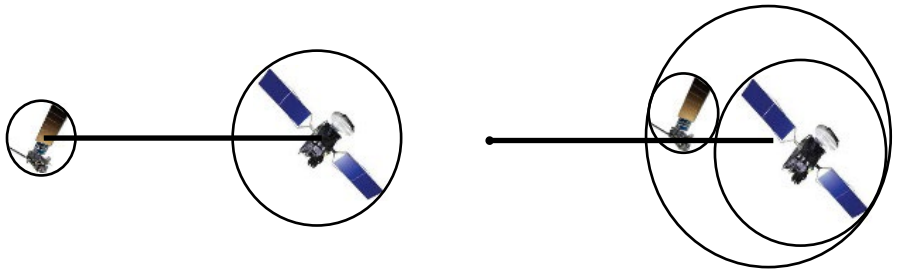

Figure N-2 Combining the Sizes of the Primary and Secondary Objects

The third step is to envision the situation at TCA in which all the uncertainty is assigned to the secondary object's end of the relative miss vector held in a fixed position in the mind. The primary object end of the relative miss vector is moving along through TCA and bringing with it the sphere representing both objects' combined size. Even though the satellites follow curved trajectories and the covariance evolves and changes at each instant, if the encounter is presumed to take place extremely quickly—and this is in most conjunctions a good assumption because the satellites' relative velocity usually exceeds 10 km/sec—then two assumptions can be made: the trajectories are essentially rectilinear during the encounter period, and the covariances (and thus the joint covariance) can be considered static. This means that the encounter can be envisioned as in Figure N-3:

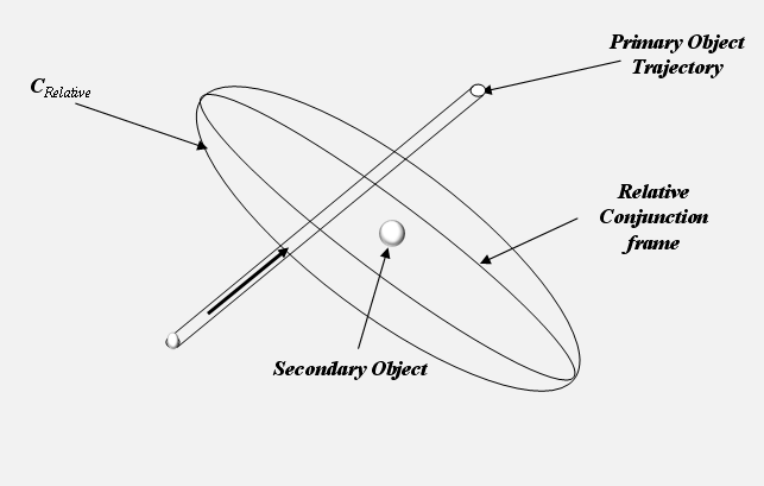

Figure N-3 Geometry at TCA

The passing of the primary object by the secondary can be seen as following a "soda straw" straight trajectory whose cylindrical radius is the same as that for the hard-body radius and whose placement is one miss distance away from the position of the secondary at TCA. Since the joint covariance shown as the ellipsoid above represents the uncertainty of one "end" of the

miss-distance vector (as shown by the central dot in the above diagram), this dot can be presumed to be potentially in any place within the ellipsoid, meaning that in some portion of those realizations, it will fall within the soda straw. When this is the case, a collision is presumed. The task is to determine the likelihood that the dot will, in the actual realization of this conjunction, fall within the cylindrical path ("soda straw") swept out by the motion of the primary object. This probability can be decomposed to be rendered as the product of the individual probabilities that each component of the secondary object position (the dot) will fall within the soda straw pathway, i.e., if an orthogonal x-y-z coordinate system is presumed, this overall probability can be generated as the product of the probability that the x-component of the dot's position will fall within the straw, the y-component of the dot's position will fall within the straw, and the z-component of the dot's position will fall within the straw. If this coordinate system is aligned so that one of the axes (e.g., the z axis) aligns with the direction of the straw, because one is assuming rectilinear motion, the soda straw can be presumed to be unbending and infinite in length, and as such, it will contain all of the z-component probability of the dot's falling within the straw. As such, the z-component probability in this arrangement will be unity and will be what is called "marginalized out," meaning that the overall probability can be fully represented by the probability remaining with the x- and y-components. The entire situation can thus be reduced from three to two dimensions and analyzed as a phenomenon that occurs on a plane that is orthogonal to the soda-straw direction, which is the direction of the relative velocity vector. This procedure defines the "conjunction plane," which can be viewed in two equivalent representations as discussed by Chan (2008, see Figure 5.1), and as shown in Figure N-4.

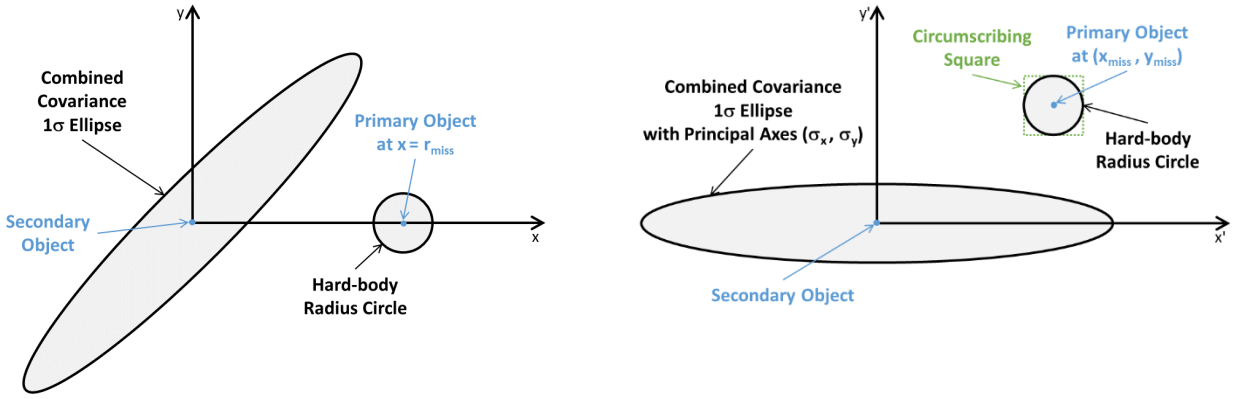

Figure N-4 Two Equivalent Representations of the Conjunction Plane

In the first representation, shown in the left panel of Figure N-4, the center of the secondary object is placed at the origin, and the local (x, y) coordinate system configured so that the miss vector (which extends a distance of r_{miss} from the secondary to the primary object) lies along the horizontal x axis. The "soda straw" is coming out of the page and represented as the hard-body-radius circle. With this planar reduction, the Pc is now the frequency with which the miss-distance vector will fall within the hard-body-radius circle; this is equivalent to the amount of joint covariance probability density (illustrated here using a 1σ ellipse) falling within that circle. Since the projected joint covariance represents a bivariate Gaussian distribution, the amount of

its probability density falling within the hard-body-radius circle is given by the following two-dimensional integral (Foster and Estes, 1992)

$$P_c = \frac{1}{\sqrt{\det(2\pi \boldsymbol{C})}} \iint_A \exp\left(-\frac{\boldsymbol{r}^T \boldsymbol{C}^{-1} \boldsymbol{r}}{2}\right) dx\, dy \qquad \text{(N-1)}$$

in which $\boldsymbol{r}$ is the 2×1 miss vector, $\boldsymbol{C}$ is the 2×2 covariance matrix, and A is the hard-body-radius circular area. There are several different approaches to evaluating this integral. Foster and Estes (1992) applied a two-dimensional quadrature technique; this works well, and MATLAB®'s[1] adaptive *quad2d* integrator is quite equal to the task, although perhaps not the most computationally efficient of all possible choices. Chan (2008) uses equivalent-area transforms to produce a single-dimensional integral, which has a series solution. Garcia-Pelayo et al. (2016) also derives a multi-term series approximation. However, even though these series approximations are relatively computationally efficient, experience indicates that they occasionally produce inaccuracies. Elrod (2019) formulates the integral in terms of complementary error functions (to improve accuracy for conjunctions with small Pc values) and uses Gauss-Chebyshev quadrature with nodal symmetry (which improves the efficiency of the numerical integration considerably). The Foster and Elrod approaches (the former being the established standard, and the latter being extremely fast, especially with a vectorized MATLAB implementation) are included as the *Pc2D_Foster* and *PcElrod* functions in the Pc Computation Software Development Kit (SDK) in the NASA CARA software repository. (See Section 7, Contact Information in this document for the specific URL.)

In the second conjunction plane representation, shown in the right panel of Figure N-4, the secondary object location again is placed at the origin, but in this case the local (x', y') coordinate system is configured so that the principal axis of the covariance ellipse lies along the horizontal axis. The center of the primary object lies at (x_{miss}, y_{miss}), and the axes are oriented so that this miss position lies within the 1st quadrant, so that $x_{miss} \geq 0$ and $y_{miss} \geq 0$. Using this representation, the Pc is given by a one-dimensional integral involving error functions (Alfano, 2005a)

$$P_c = \frac{1}{\sqrt{8\pi}\sigma_x} \int_{-R}^{R} \{\mathrm{erf}(y_+) - \mathrm{erf}(y_-)\} \exp\left[-\frac{(u + x_{miss})^2}{2\sigma_x^2}\right] du \qquad \text{(N-2)}$$

with R indicating the combined hard-body radius, $u = x' - x_{miss}$ the integration variable, and $y_\pm = (y_{miss} \pm \sqrt{R^2 - u^2})/(\sqrt{2}\sigma_y)$. The integrand factor in the curly brackets represents the difference of two error functions, $\Delta = -\mathrm{erf}(y_-)$. In many software environments (e.g., MATLAB), this factor often can be computed significantly more accurately as a difference of complementary error functions, i.e., $\Delta = \mathrm{erfc}(y_-) - \mathrm{erfc}(y_+)$, especially when calculating very small Pc values (Elrod, 2019). See Abramowitz and Stegun (1970) and Press et al. (1992) for details on computing erf(-) and erfc(-) functions.

For most conjunctions, Gauss-Chebyshev quadrature provides an efficient and accurate means to calculate the one-dimensional integral in equation (N-2), using an approach similar to that

[1] MATLAB is a registered trademark of The MathWorks, Inc.

described by Elrod (2019). However, for conjunctions involving relatively large hard-body radii (or, equivalently, small covariance ellipse σ_x dimensions), this method can potentially become inaccurate. Specifically, Gauss-Chebyshev quadrature becomes increasingly inaccurate as the hard-body radius grows beyond the limit $R_{lim} = 4\sigma_x - \min(R)$. In such cases, which rarely occur in practice, an adaptive numerical integrator can be used to calculate an accurate estimate, e.g., MATLAB's *integral* function. (The function *PcConjPlaneCircle* of the NASA CARA SDK repository implements a vectorized algorithm that automatically determines which of these two integration methods should be used to compute Pc values accurately for all input hard-body radii and covariance values, with a computation speed comparable to that of the *PcElrod* function for most conjunctions. Also, for cases that have hard-body radii well below the limit given above, testing indicates that the SDK functions *Pc_Foster*, *PcElrod*, and *PcConjPlaneCircle* all output nearly identical numerical Pc values, i.e., that typically agree to five digits of precision or more.)

The second conjunction plane representation shown in the right panel of Figure N-4 also provides an extremely efficient means to calculate an upper limit estimate for the Pc value. This upper bound corresponds to the two-dimensional (2-D) integral over the square that circumscribes the hard-body radius circle (as shown in Figure N-4), which has the following analytical solution

$$P_c < P_{sq} = \frac{[\mathrm{erf}(X_+) - \mathrm{erf}(X_-)]\,[\mathrm{erf}(Y_+) - \mathrm{erf}(Y_-)]}{4} \tag{N-3}$$

with

$$X_\pm = \frac{x_{miss} \pm R}{\sqrt{2}\sigma_x} \quad \text{and} \quad Y_\pm = \frac{y_{miss} \pm R}{\sqrt{2}\sigma_y} \tag{N-4}$$

Again, in many cases the erf(-) differences in equation (N-3) can be computed more accurately using erfc(-) differences. Notably, the circumscribing square probability estimate does not require any numerical integration at all, but instead only requires the computation of four erf(-) or erfc(-) functions, usually making it relatively easy to program into software and significantly more computationally efficient. These considerations could be important in some circumstances (e.g., for computations performed on orbiting satellites), prompting the use of P_{sq} as an approximation for P_c itself. For instance, CDMs generated by the USSPACECOM ASW processing system often reports P_{sq} as the estimate of conjunction's collision probability. (An optional, non-default mode of the function *PcConjPlaneCircle* in the NASA CARA SDK repository implements an efficient vectorized algorithm that calculates P_{sq} values).

It is perhaps helpful at this point to review the four assumptions employed by the conjunction plane Pc calculation methods given by equations (N-1) through (N-4), because alternative Pc estimation techniques will be needed when these assumptions do not inhere:

1. Statistical Independence: The two objects' uncertainty distributions are statistically independent so that the joint covariance can be obtained by simple addition of the two covariances. This assumption is largely true but can break down for objects that share global atmospheric density forecast error in a manner that influences the conjunction. This issue will be discussed as an isolated topic in a subsequent section of this appendix.

2. Rectilinear Motion: The conjunction circumstances are such that it is reasonable to presume rectilinear motion and static covariances during the encounter. These conditions inhere for most conjunctions between Earth-orbiting satellites. The objects' relative velocity at TCA is in some places used as an indication of the reasonability of these assumptions, but this parameter alone is not sufficient to identify situations in which the conjunction plane Pc approximation will miscarry.
3. Gaussian Position Distributions and Negligible Velocity Uncertainties: The position vector state errors for each satellite at TCA follow Gaussian distributions, and the velocity vector state errors are negligibly small. When combined, these assumptions lead to the conjunction plane representations shown in Figure N-4. Conjunctions that do not satisfy these assumptions are addressed by alternate analytical and Monte Carlo methods, discussed in the sections below.
4. Temporally Isolated Event: The conjunction presents a single, well-defined event so that the collision likelihood can be ascertained by examining that single instance. Objects that stay in close proximity for extended periods accumulate risk throughout long interactions, rather than quickly accumulating risk at or near a well-defined TCA. A different approach is also required for their evaluation, which is discussed in the sections below.

As mentioned previously, the issue of statistical independence (i.e., assumption 1 above) will be discussed in a subsequent section of this appendix. To address conjunctions that do not satisfy any of the other assumptions, two alternative (but more computationally intensive) analytical methods are available: the "three-dimensional Nc" method, which research indicates can be applied to conjunctions that violate assumptions 2, 3 and/or 4 above, and the "two-dimensional Nc" method, applicable to temporally isolated conjunctions that violate assumptions 2 and/or 3. Notably, the three-dimensional Nc method could, in principal, be applied to all conjunctions to estimate Pc values. However, this is not justified because most LEO satellite conjunction Pc values can be estimated accurately using the much more efficient conjunction plane methods described above. Additionally, most of the remaining conjunctions can be estimated accurately using the two-dimensional Nc method, which, although much slower than the conjunction plane methods, is still significantly faster than the full three-dimensional Nc method. (The function *PcConjPlaneUsageViolation* soon to be posted on the NASA CARA Software Development Kit (SDK) repository provides an algorithm that determines if a given conjunction violates one or more of conjunction plane Pc estimation assumptions, and if so, which of the other available Pc estimation methods are appropriate.)

N.3 Three-Dimensional Nc Method Analytic Pc Calculations

The relatively infrequent conjunctions that do not satisfy the conjunction plane method assumptions discussed in the previous section must be addressed with a different methodology, and in response to this need, several authors have formulated semi-analytical approaches relaxing some or all of these assumptions. Coppola (2012) proposed a method for single encounters designed to account for non-linear orbital motion and velocity uncertainties, resulting in an approximation for the probability rate, $\dot{P}_c(t)$, calculated using integration over the surface of a unit sphere. When combined with a one-dimensional time integration, this yields a "three-

dimensional Pc" approximation. Chan (2015) contested Coppola's formulation, arguing that a proper approach must employ a set of random variables associated with a time-invariant Probability Density Function (PDF). NASA CARA implemented the three-dimensional Pc method in software (Hall et al. 2017a) and subsequently discovered that, for some conjunctions, it can produce P_c estimates that differ significantly from high-fidelity Monte Carlo Pc calculations, even though all the required three-dimensional Pc assumptions are satisfied.

Shelton and Junkins (2019) provided a key insight into why the original three-dimensional Pc approximation fails in certain situations. Their analysis indicates that accurate Pc approximations require that the state uncertainty PDFs of the two satellites be estimated accurately *in the volume of space where they overlap the most*. The original Coppola (2012) three-dimensional Pc formulation did not incorporate this concept, but Hall (2021) reformulated the method to do so explicitly. For single encounters, the reformulated approach approximates the curvilinear motion of each satellite using a first-order Taylor series expansion, not centered on the mean orbital state, but centered instead on a state that coincides with the maximum overlap of the PDFs for the two satellites. The analysis demonstrates that such "peak overlap" states can be determined using an iterative calculation that converges quickly. The formulation derives an expression for "Nc" — the statistically expected number of collisions — which equals Pc for single, temporally isolated conjunctions, but that may exceed Pc for multi-encounter interactions. The resulting "three-dimensional Nc" method entails a total of three numerical integrations, one over time and two over the surface of a sphere. The outermost, time integration expression has the form

$$N_c(\tau_a, \tau_b) = \int_{\tau_a}^{\tau_b} \dot{N}_c(t)\, dt \tag{N-5}$$

This expression estimates $N_c(\tau_a, \tau_b)$, the number of collisions statistically expected to occur at some time during the risk assessment interval $\tau_a \leq t < \tau_b$, which can represent either a short duration closely bracketing a single close-approach encounter, or an extended duration spanning multiple encounters. The expected collision number is closely related to the collision probability. In fact, they are equal for single, isolated encounters between well-tracked satellites. The collision rate for such a temporally isolated conjunction is expressed as a two-dimensional integral over the unit sphere

$$\dot{N}_c(t) = R^2 \int_0^{2\pi} \int_0^{\pi} \left[\nu_t(\hat{\boldsymbol{r}})\, MVN\left(R\hat{\boldsymbol{r}}, \breve{\boldsymbol{r}}_t, \widetilde{\boldsymbol{A}}_t\right)\right] \sin(\theta)\, d\theta\, d\varphi \tag{N-6}$$

In this equation, the radial unit vector is given by $\hat{\boldsymbol{r}} = [\cos(\varphi)\sin(\theta), \sin(\varphi)\sin(\theta), \cos(\theta)]^T$, so the surface of the unit sphere is spanned by the azimuthal angle $0 \leq \varphi < 2\pi$ and the axial angle $0 \leq \theta \leq \pi$. The leading factor of R^2 represents the square of the combined hard-body radius, meaning that the expression actually represents an integration over the surface area of the collision sphere. As explained in Hall (2021), the integrand function in the square brackets is the product of two factors. The first in an average velocity term, $\nu_t(\hat{\boldsymbol{r}})$, which is a function of time (as indicated by the *t* subscript) and calculated using the TCA states and covariances of the primary and secondary objects. The second factor, $MVN(R\hat{\boldsymbol{r}}, \breve{\boldsymbol{r}}_t, \widetilde{\boldsymbol{A}}_t)$, represents a multi-variate

normal (MVN) function which depends on $\hat{\boldsymbol{r}}$ and R, as well as a 3×1 relative position/velocity state vector, $\check{\boldsymbol{r}}_t$, and an associated 3×3 $\widetilde{\boldsymbol{A}}_t$ covariance matrix, both of which are also calculated from the TCA states and covariances. Lebedev quadrature (Lebedev and Laikov, 1999) provides an efficient method for numerical integration over the unit sphere. (The function *Pc3D_Hall* of the NASA CARA SDK repository computes conjunction Pc estimates, along with associated Nc and Nc rate estimates, using the Hall (2021) three-dimensional Nc method as summarized in equations (N-5) and (N-6) above.)

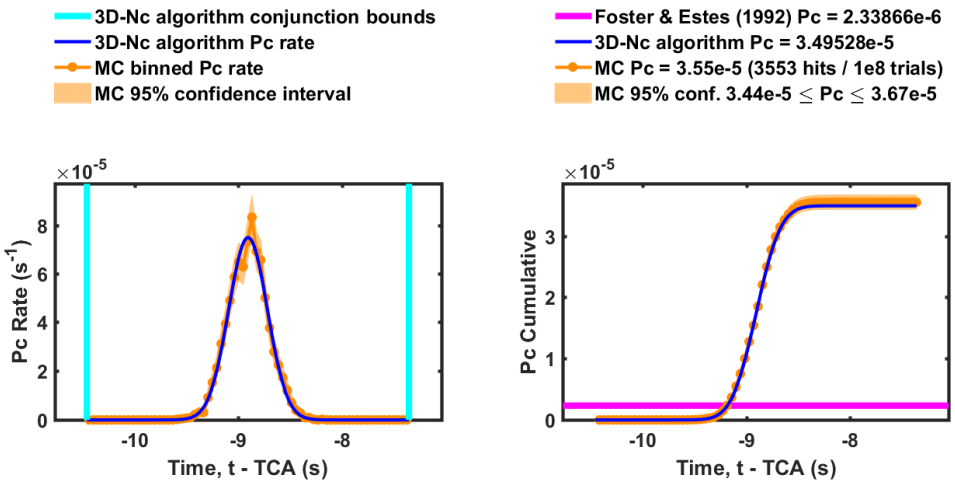

Figure N-5 Pc Rate and Cumulative Pc for a Non-Rectilinear Conjunction

Figure N-5 shows the time-dependent collision rate (left) and the cumulative Pc (right) calculated using the three-dimensional Nc method, as applied to an archived CARA conjunction that has a high relative velocity (~13 km/s), but that fails to satisfy the rectilinear motion and Gaussian PDF assumptions. This specific event does not satisfy these assumptions because it involves an object in a highly eccentric orbit with a conjunction occurring in the relatively tightly curved part of the trajectory near perigee, a phenomenology discussed by Hall (2018). In this case, the three-dimensional Nc method calculates a Pc value which accurately matches the Monte Carlo from TCA method Pc estimate, but that is a factor of fifteen larger than the erroneous conjunction plane Pc estimate, calculated in this case using the two-dimensional Foster and Estes (1992) method. It is of interest that the peak point of risk accumulation occurs nine seconds before the TCA, with essentially all the risk accumulated by 8 seconds before TCA. Such a result can seem counterintuitive at first, for one would initially expect that the point of highest risk would always be at the TCA. However, what is operative is the alignment between the geometric miss distance and the covariance. If at TCA very little of the position uncertainty lies along the relative miss vector, then that miss vector is a strong statement of the actual miss; and if the vector is somewhat larger than the hard-body radius (HBR), then the collision risk at that point is quite low. If, however, somewhat earlier or later than TCA the combined covariance (which, it must be remembered, is constantly changing position) does more substantially align along the miss vector, then more possible instantiations of the true miss are likely to be smaller than the HBR (even with the nominal miss vector larger than the expected miss at TCA), so the risk at that point is actually higher. In the more extreme cases, such as that shown in the above example (and even more strongly in the one below), most of the risk accumulation can be

relatively far from TCA, meaning that methods that examine the situation only at TCA can misrepresent this risk.

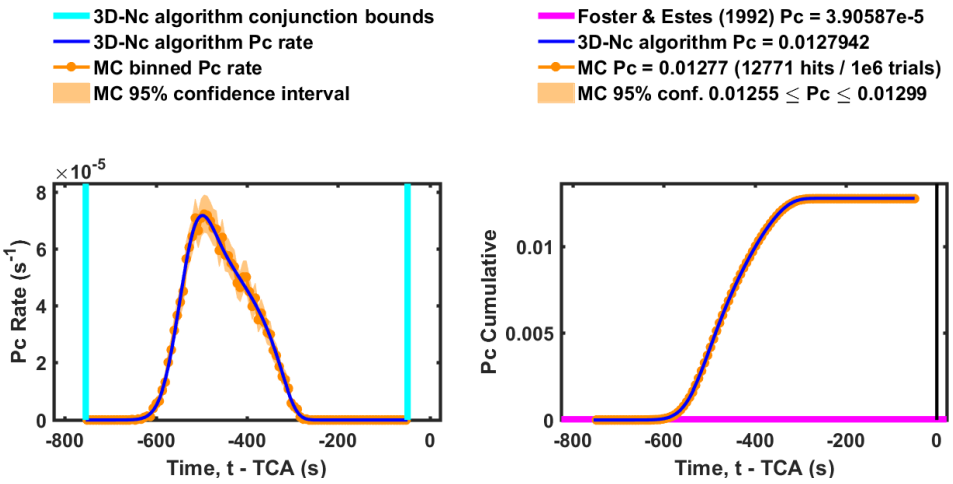

Figure N-6 Pc Rate and Cumulative Pc for a Low Velocity Conjunction

Figure N-6 shows the collision rate (left) and the cumulative Pc (right) for low relative velocity conjunction (~3 m/s), that fails to satisfy the rectilinear motion, temporally isolated, and Gaussian PDF assumptions. In this case, the three-dimensional Nc algorithm estimates a Pc value which matches the Monte Carlo from TCA method Pc estimate, but that is a factor of 330 larger than the erroneous conjunction plane Pc estimate.

N.4 Two-dimensional Nc Method Analytic Pc Calculations

As formulated in equations (N-5) and (N-6), the three-dimensional Nc method requires the computation of a time-series of many unit-sphere integrations, each calculated using Lebedev quadrature. However, as described by Hall et al. (2023), for temporally isolated conjunctions (i.e., those that are not too "extended" or "blended" in time as described by Hall 2021), the integration over time can be approximated analytically, ultimately yielding a single unit-sphere integral. This relatively efficient "two-dimensional Nc" (or 2D-Nc) method yields accurate Pc estimates for high velocity, temporally isolated conjunctions that are affected significantly by curvilinear trajectory effects (such as the example shown in Figure N-5). However, 2D-Nc is not applicable to some low velocity events that are too temporally extended or blended (as shown in Figure N-6); these kind of conjunctions still require the use of the three-dimensional Nc method or Monte Carlo estimation. The function *Pc2D_Hall* of the NASA CARA SDK repository computes Pc estimates for temporally isolated conjunctions using the two-dimensional Nc method.

Hall et al. (2023) describe a multistep algorithm that uses the semi-analytical 2D-Pc, 2D-Nc, and 3D-Nc methods along with the from-TCA and from-epoch Monte Carlo methods, in order to calculate accurate Pc values regardless whether they are affected by curvilinear trajectory effects or by low-velocity encounters. The multistep algorithm sequentially applies these five increasingly accurate Pc estimation methods, but only as required to ensure computational efficiency, by conservatively evaluating potential usage violations for each.

N.5 Comparison of Pc Estimates for Temporally Isolated Conjunctions

Figure N-7 shows a comparison of collision probabilities for 63,603 temporally isolated conjunctions extracted from the NASA CARA database for the period 2017-05-01 and 2019-08-15 and for events with 2D $P_c > 10^{-7}$ (Hall, 2021). The vertical axes on all three panels plot Monte Carlo (MC) estimates for the collision probability—specifically, Monte Carlo from TCA method Pc estimates, which are also referred to in this figure as two-body Monte Carlo method Pc estimates (i.e., TBMC-Pc estimates, as described in more detail in section N.13). The error bars in Figure N-7 show 95% confidence intervals estimated using the Clopper-Pearson method (1934); several of the conjunctions had zero hits registered in the Monte Carlo simulations, which are represented in Figure N-7 using downward-pointing triangles and a single-sided error bar. The horizontal axes plot the corresponding semi-analytical approximations: two-dimensional Pc on the left graph, three-dimensional Nc in the center, and two-dimensional Nc on the right. The colored points on each plot indicate the results of a binomial proportion statistical test that evaluates the agreement between the estimates. Specifically, black points in Figure N-7 indicate analytical Pc estimates that agree reasonably well with the Monte Carlo estimates as they do not violate a null-hypothesis that the two are equal at a p-value $\leq 10^{-3}$ significance level. However, those highlighted in yellow do violate the hypothesis at this significance level, and those in red at a more stringent level of p-value $\leq 10^{-6}$. Overall, the two-dimensional conjunction plane Pc comparison plotted in the left graph contains 254 yellow and 436 red points, which both significantly exceed the number of disagreements expected from purely statistical variations, even though together they represent a small fraction (~1%) of the original conjunctions. These disagreements represent conjunctions that violate one or more of the assumptions required for conjunction plane Pc estimation. The center graph clearly shows that the three-dimensional Nc method matches the Monte Carlo Pc estimates better, producing only 66 yellow and zero red points. Finally, the two-dimensional Nc method plotted on the right produces very nearly the same results as the three-dimensional Nc method but requires much less computation time. The three comparisons shown in Figure N-7 indicate that, for temporally isolated conjunctions, the two- and three-dimensional Nc methods are consistent with one another and match Monte Carlo Pc estimates significantly better than the conjunction plane Pc estimation method.

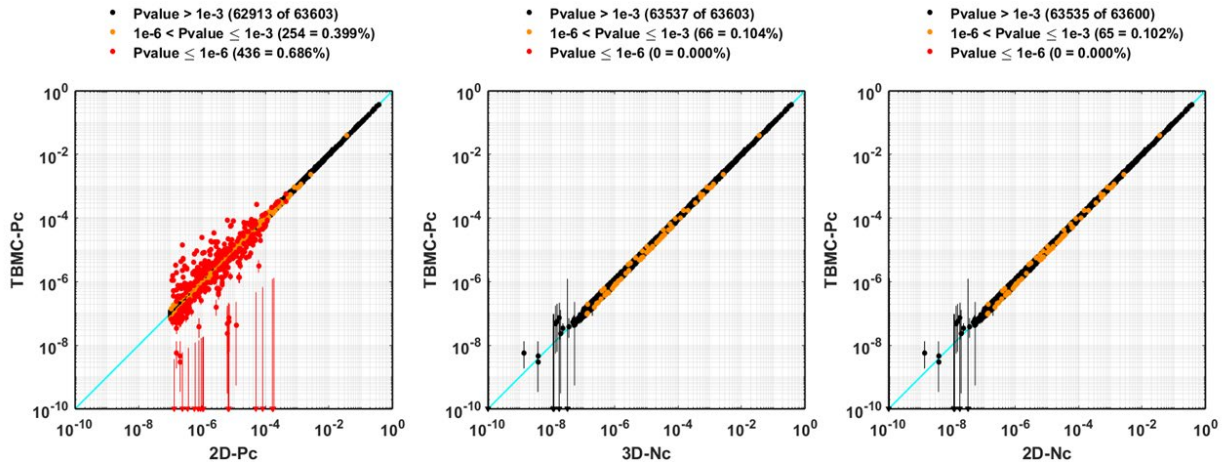

Figure N-7 Comparison of Monte Carlo Collision Probabilities with the Two-Dimensional P_c Method (left), the Three-Dimensional N_c Method (center), and the Two-Dimensional N_c Method (right) for a Large Set of CARA Conjunctions

N.6 Pc Calculations for Multi-encounter Interactions

An additional feature of the two- and three-dimensional Nc methods is their ability to address explicitly the amalgamated risk of repeating conjunctions. While most conjunctions are temporally isolated, there are two conjunction types that exhibit different behaviors. The first type is produced by objects in orbits in synodic alignment that generate a temporal sequence of conjunctions once every revolution or multiple of a revolution (e.g., two nearly circular orbits at different inclinations that produce conjunctions at one or both nodal crossing points). The second type involves objects that orbit close to each other for extended periods, generating extended interactions with multiple close approaches (e.g., two satellites in nearly the same orbit, but with only a slight difference in inclination and/or eccentricity). In both cases, if each of the multiple encounters is considered separately, situations can arise in which each encounter in the series falls below a Pc mitigation threshold, but the combined risk of all of the encounters exceeds that threshold. The two- and three-dimensional Nc methods account for such multi-encounter interactions by providing estimates for the total expected number of collisions, and upper and lower bounds for the probability of collision (Hall, 2021; Hall et al., 2023). The total statistically expected number of collisions for a multi-encounter interaction is given by a summation of Nc values for each conjunction in the sequence

$$N_c(\tau_a, \tau_b) = \sum_{k=1}^{K} N_{c,k} \tag{N-7}$$

with the index $k = 1 \ldots K$ indicating the close approaches applicable to the risk assessment interval $\tau_a \leq t < \tau_b$, and $N_{c,k}$ representing the associated expected number of collisions for each. The upper and lower Pc bounds for the combined interaction are given by

$$\max\left(N_{c,k}\right) \leq P_c(\tau_a, \tau_b) \leq 1 - \prod_{k=1}^{K}(1 - N_{c,k}) \tag{N-8}$$

which also implies that $P_c(\tau_a, \tau_b) \leq N_c(\tau_a, \tau_b)$. Figure N-8 shows an example of a multi-encounter interaction, in which a pair of satellites experience four conjunction events over about a five-hour period. Each of the individual conjunctions produces a Pc value in the upper yellow region (between 10^{-5} and 10^{-4}), as plotted in the bottom panel. The solid line in the top panel shows the upper limit of the cumulative Pc for the interaction; notably, after the third conjunction, the cumulative Pc exceeds 10^{-4} — a value frequently selected as a risk mitigation threshold. So, while these events would not necessarily prompt a mitigation action if examined individually, when considered collectively they do appear to represent a situation of sufficiently high collision likelihood to warrant mitigation. In such a case, it is advisable to run a Monte Carlo investigation (discussed in a subsequent section of this appendix) to verify that the upper-

limit Pc value generated by the method is in fact representative of the actual cumulative risk. The utility of the analytic calculation, however, should be clear: if the upper-bound calculation for repeating events is found to be below the mitigation threshold, then there is no need to marshal computationally intensive methods (such as Monte Carlo), for it has already been demonstrated no mitigation action is warranted.

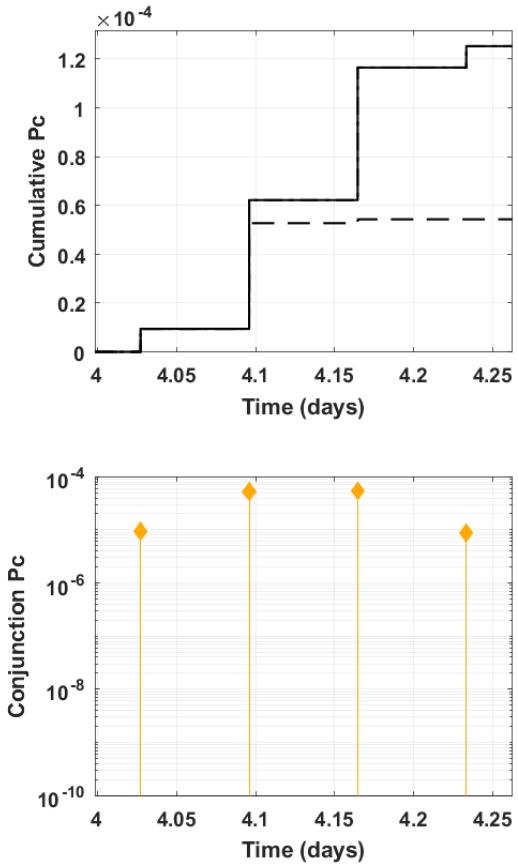

Figure N-8 Cumulative Three-Dimensional N_c Risk Over Four Repeating Conjunctions

N.7 Input Covariance Data Considerations

Most calculations are only as good as the input data that drive them, and Pc calculation is no exception. Appendix P discusses orbit determination quality and propagation issues for individual objects and addresses the question of the circumstances under which the state estimate and covariance might be considered sufficiently poor so as not to constitute a basis for conjunction risk mitigation actions. The purpose of this section is to address the routine improvement and basic error checking extended to covariances as part of the Pc calculation. These activities fall into three basic groups: correction for known problems in propagation, covariance formation and stability issues, and correlation between primary and secondary covariances. Each of these topics will be treated in turn.

N.7.1 Propagation Error Compensation

Historically, accuracy analysis of state estimate and uncertainty estimates has focused on products that emerge directly from the orbit determination fit. These direct orbit-determination products include best-estimate states and covariances of the satellite at an epoch that usually coincides with the acquisition time of the last tracking metric observation incorporated into the analysis. While these direct orbit-determination products are of course foundational, it is important to remember that most SSA activities, and conjunction assessment in particular, are not usually conducted with these direct products but rather with predictions propagated from the orbit-determination epoch solution, often over a non-trivial duration that spans many orbital revolutions into the future. The batch orbit-determination analysis method used by the DOD produces a formation covariance that represents the expected at-epoch state uncertainty based on the number, quantity, and temporal spacing of the incorporated metric observations; when the state is propagated forward, a parallel process can also be used to propagate the covariance forward in time. The same dynamical models used for the orbit-determination analysis as well as the state propagation itself are used to perform this covariance propagation, although in a linearized way. This means that the propagated covariance will be sized (mostly) appropriately for both the propagation duration and the final prediction point in the orbit.

Despite the use of appropriate models to propagate the covariance forward in time, a number of additional sources of error manifest themselves during the propagation interval yet are not part of the dynamical model used during the fit; these errors are therefore neither incorporated into the orbit-determination-produced covariance nor added as part of the regular propagation process. Because of the prevalence of such outside-of-model errors, techniques have been developed to account for them, the most familiar of which is the addition of process noise during propagation. Originally developed to account for acceleration errors that, due to model inadequacy, were to some degree known, this method propagates a noise matrix alongside the propagated covariance and combines both matrices as part of the overall process. The result is a covariance that is larger than it would have been otherwise to account for these (characterized) errors in the force model(s). A second approach, which is the one used by DOD in the propagation of their orbit prediction products, applies parameters to the covariance before propagation to guide the propagation process in producing a more realistic result. Because this is the approach reflected in the CDM covariances that conjunction assessment practitioners receive from the DOD, it will be described here in some detail.

Orbit determination makes a distinction between “solved-for” parameters that are actually estimated during an orbit-determination activity, and “consider” parameters that are not “solved for” but represent *a priori* information that is “considered” as part of the orbit-determination process. In the present case, the use of the term “consider parameter” is somewhat non-nominal in that it is referring not to additions or alterations made during the fit but to modifications to the fit-produced covariance so that when it is propagated, it may give a more realistic representation of the expected state errors. For DOD covariances, two different consider parameters are applied to compensate for two distinct expected errors during propagation: atmospheric density forecast error and satellite frontal area uncertainty.

Atmospheric drag is a significant force that affects satellite orbits with perigee heights less than 1000 km, and the calculation of the expected atmospheric drag at any particular moment requires an estimate of the neutral atmospheric density that that satellite will encounter at that moment. Because the atmospheric models that generate this estimate are driven by space weather indices, the ability to predict these indices accurately affects the fidelity of the predicted atmospheric density and thus the atmospheric drag. Unfortunately, it is difficult to predict future space weather indices well, primarily because they are affected by activities on the part of the sun's surface that has not yet rotated into view from the Earth. This particular issue was studied with the Jacchia-Bowman High Accuracy Satellite Drag Model (HASDM) 2009, which is the atmospheric density model used by DOD, by comparing predicted densities (using predicted space weather indices) to actual densities and producing polynomial fits of the relative density error as a function of satellite perigee height and the Ap (major magnetic storms list) and Dst (disturbance storm-time) space weather indices. Figure N-9 shows the behavior of these polynomial fits divided into four different classes of Ap/Dst activity; y-axis values are omitted here to allow full releasability of the figure:

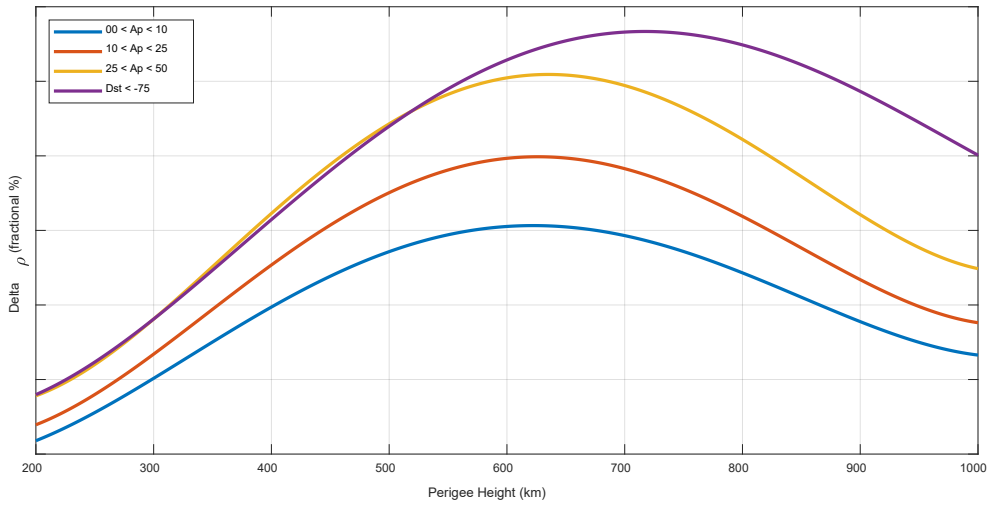

Figure N-9 Behavior of Relative Density Error by Perigee Height and Solar Activity

These fits produce a variance term that can be added to the ballistic coefficient variance in the covariance: because in the drag equation the ballistic coefficient and the atmospheric density estimate are multiplicatively coupled, changing one of these parameters has the same effect as changing the other. When the covariance is propagated, this augmented term will appropriately expand the other covariance terms.

The amount of drag acceleration a satellite encounters is also governed by the frontal area that the satellite presents to the atmosphere; this makes intuitive sense (amount of resistance is a function of area presented to the resisting fluid) and is reflected in the ballistic coefficient (B) equation

$$B = C_D \frac{A}{M} \qquad \text{(N-9)}$$

in which C_D is the (dimensionless) drag coefficient, which indicates the degree to which the satellite surface is susceptible to drag resistance; M is the satellite mass; and A is the satellite frontal area. As A increases, B increases as well, increasing the overall drag acceleration value. Stabilized satellites should manifest a stable B term, but rotating satellites, because their frontal area term is continuously changing, can exhibit a range of B terms. Three outcomes are possible depending on the rapidity of the rotation: the effect can be washed out during the fit (because the rotation is so rapid that an average value is quite representative), the effect can be not relevant during the fit (because the rotation is so slow that it does not affect near-term look-back and look-forward), or the effect can be such that the rotation does affect results fit-to-fit. It is this last case for which compensation is helpful. A history of regularized B histories for individual satellites is examined and a relative error and variance calculated, and this variance is added to the drag variance in the covariance as a corrective term whose influence will be realized in propagation.

There is some additional subtlety regarding the exact way these consider parameters are applied. A typical propagation consists of two conceptual stages: the first stage is the propagation forward from the epoch time of the orbit determination to the present time, which can make use of measured and thus highly reliable space weather indices; and the second stage is from the present time to the desired final propagation time, which has to use predicted space weather indices and the errors that these introduce. The two consider parameters are thus applied at different times. Because satellite rotation and its resultant uncertainty will occur for the entire interval from epoch time to the propagation end point, that consider parameter is applied at epoch. Atmospheric density forecast error, however, is encountered only forward in time from the present moment, so it is added only for that portion of the propagation. Figure N-10 outlines the two-phase application of these consider parameters:

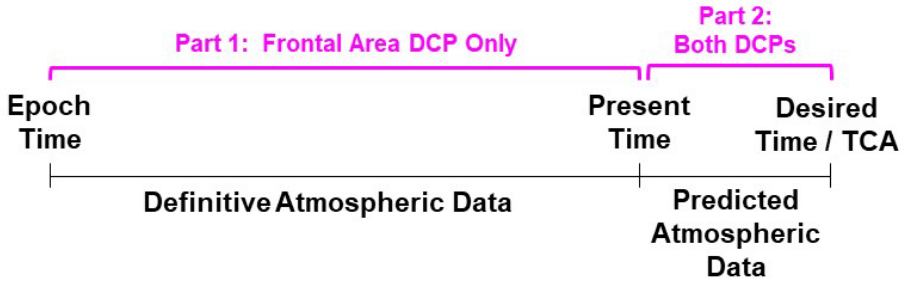

DCP = Dynamic Consider Parameter

Figure N-10 Two-phase Application of Consider Parameters

If the CDMs generated by the DOD are used for conjunction assessment applications, the good news is that all the consider parameter activities described above are already performed—the propagated covariances that the CDM contains have had these two consider parameters applied during the covariance propagation executed at the DOD work center. If one is working with

epoch state estimates, which is sometimes necessary when performing Pc calculations with Monte Carlo techniques, then manual application of the consider parameters may be necessary. This issue is discussed at greater length in the section that addresses Monte Carlo Pc calculations.

N.7.2 Defective Covariances

There are several ways in which a covariance contained in a CDM can be defective.

- **Null Covariances**. All-zero, or null, covariances are sometimes observed, usually arising from a conjunction assessment screening for which the O/O-provided ephemeris does not contain covariance data. In such a case, it is possible to compute the Pc either using only the one covariance that the CDM message contains or by applying a special technique that determines the maximum Pc possible presuming that the null covariance could take on any possible value (developed and described in Frisbee 2015).
- **Default Covariances**. Default covariances are diagonal covariances that contain a value of ten earth radii squared for each of the three position variances. The presence of this covariance indicates that a precision, special-perturbation solution for the object was not possible; the state estimate provided arose from a general-perturbation solution, and an orbit-determination-produced covariance was not available. Such a result is not a precision solution and does not constitute a basis for conjunction risk mitigation actions.
- **Non-Positive-Semidefinite Covariances**. Another defective covariance type found in CDMs, now quite rare due to improvements to the DOD operational system, is a covariance that fails to be positive semidefinite. A positive semidefinite matrix is one that contains no negative eigenvalues. Because the covariance represents a hyperellipsoid of actual state error information, it must have a set of eigenvalues all greater than or equal to zero for error information to consist of real rather than imaginary quantities. The orbit-determination mechanism that generates the covariance should always produce at least a positive semidefinite matrix, for the linear algebra function involves the product of a square matrix and its transpose, and one can prove that this procedure always produces a positive semidefinite result. Due to either numerical precision limits or interpolation, the provided matrix is sometimes not positive semidefinite. If the 2 × 2 projection of the covariance matrix into the conjunction plane is not positive semidefinite, the two-dimensional Pc calculation is not possible. If the full 6 × 6 or 8 × 8 matrix is not positive semidefinite, then Monte Carlo sampling on the entire matrix is not possible either.

As such, some attention must be paid to this issue of positive semidefinite matrix conditioning. A recent paper on this subject (Hall 2017b) examined the issue in some detail and compared different matrix repair algorithms to minimally adjust the covariance to make it positive semidefinite compliant; it found that most repair approaches yield equivalent answers in terms of the resultant calculated Pc. An “eigenvalue clipping” procedure was developed in which any negative eigenvalues (which are almost always small) are set to a small positive or zero value, as required.

The CARA operational implementation of this method proceeds parsimoniously, namely by directing such repair only to the level needed to perform a calculation. For example, a covariance used for the two-dimensional Pc calculation would neither be tested for positive semidefinite compliance in its full 8 x 8 form nor its position-only 3 x 3 form; instead, the 2 x 2 projection of the joint covariance into the conjunction plane would be tested and repaired only when necessary to enable the two-dimensional Pc calculation. To do otherwise is to make repairs and potentially alter the result when this is not strictly necessary.

The Pc Computation CARA SDK includes the source code for identifying the need for and making the covariance matrix repairs described above; it is available in the NASA CARA software repository. (See Section 7, Contact Information in this document for the specific URL.)

N.7.3 Covariance Correlation

For nearly all the broader conjunction assessment conduct during the past decade, practitioners operated with the presumption that the primary and secondary objects' covariances could be considered uncorrelated. Not only was this the "right" answer in that it greatly simplified the Pc computation because the joint covariance could be formed by simple addition of the two covariances, but there was also a good intuitive justification for the presumption. Because the focus had been on the two objects' orbit-determination fits, which are based on separate sets of observations, there was no expectation that there would exist any significant correlation between the two objects' covariances. The principal source of potentially correlated error was presumed to be uncharacterized but correlated errors in space sensor observations used by both primary and secondary objects. Because most primaries receive many observations from many different sensors, it was seen as unlikely that this particular source would introduce much correlation. Correlation between covariances was thus expected to be small, and conjunction assessment operators proceeded as though it were.

With the initiative several years ago to include outside-of-fit prediction error characterization into DOD satellite covariances (see the above section on Propagation Error Compensation), the issue of covariance cross-correlation began to be rethought. The principal outside-of-fit prediction error is global atmospheric density forecast error due to inadequate space weather index prediction. Because this is a global error, it is likely to be shared among large classes of objects, some of which might constitute both the primary and secondary objects in a conjunction. As discussed previously, this global density forecast error has been parameterized by satellite perigee height and predicted geomagnetic index, so the degree of such error, both identified separately and injected into each DOD-furnished covariance by means of a consider parameter, is known for each satellite. It is possible to determine the degree of shared error from this source and account for it when forming the joint covariance.

A study by Casali et al. (2018) provides a full development of this theory and presents results for an evaluation set of conjunction data. Essentially, one has to determine the global density forecast error relevant to each satellite and the degree to which the associated drag error induced by this density forecast error will manifest itself in position error relevant to the particular conjunction. The governing equation is the following:

$$P_m = P_s + P_p - \sigma_{s/g}\,\sigma_{p/g}\,G_s\,G^T_p - \sigma_{s/g}\,\sigma_{p/g}\,G_p\,G^T_s \qquad \text{(N-10)}$$

in which P_m is the decorrelated joint covariance at TCA, P_s is the secondary covariance at TCA, P_p is the primary covariance at TCA, $\sigma_{s/g}$ is the density forecast error germane to the secondary satellite, $\sigma_{p/g}$ is the density forecast error germane to the primary satellite, G_s is the sensitivity vector mapping drag acceleration error to secondary satellite position error at TCA, and G_p is the sensitivity vector mapping drag acceleration error to primary satellite position error at TCA. One could wonder how the conjunction assessment practitioner would come upon all of the needed data to effect the proposed compensation. As described in detail in the next section, a recent enhancement to the DOD operational system has placed all of this information in the CDM itself, allowing the direct calculation of the decorrelated joint covariance. The CARA Pc Calculation SDK, available on the NASA CARA software repository, also contains both a math specification outlining this calculation and source code to perform it. (See Section 7, Contact Information in this document for the URL.) Hall (2021) describes how the density forecast errors and sensitivity vectors can be used to estimate decorrelated joint covariances for the two- and three-dimensional Nc methods.

A heuristic probing of the situation reveals that, conjunction by conjunction, different levels of Pc changes are possible due to cross-correlation remediation. Orbits that are insensitive to atmospheric drag are little affected by density forecast error and will have Pc estimates that, as expected, also change little. Head-on conjunctions are expected to be left mostly unaffected as well, for the components of the error that govern the Pc are not subject to density forecast error perturbation. Crossing events are perhaps the most susceptible to cross-correlation effects, especially if the drag level of both satellites is similar.

The plot in Figure N-11 profiles 250 conjunctions in which the primary and secondary satellites are of non-negligible drag (i.e., Energy Dissipation Rate (EDR) values greater than 0.0006 watts/kg; see Hejduk 2008 for an explanation of energy dissipation rate) and plots the ratio of the Pc calculated with the decorrelated joint covariance to that of the Pc calculated with the unmodified joint covariance. One can see that for somewhat more than half of the events, the ratio hovers near unity, meaning that the conjunction is little affected by the compensation. For about one-third of the cases, the decrease in Pc is notable, in many instances more than an order of magnitude. For the remaining cases, there is an increase in Pc from a factor of 1.5 to 5.

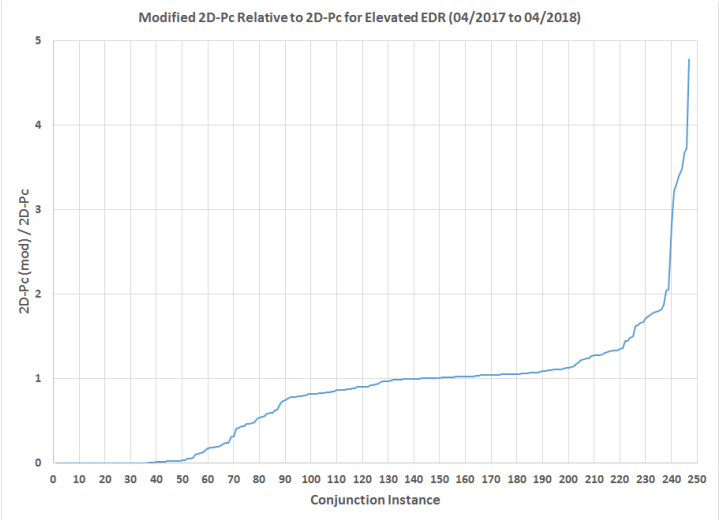

Figure N-11 Profiles of 250 Conjunctions with Primary and Secondary Satellites of Non-negligible Drag[2]

While the Pc value changes by less than a factor of 1.5 for most of the conjunctions, a sufficient number are affected more substantially therefore justifying the integration of this additional consideration into the Pc computation, especially because it is a straightforward calculation from data provided directly in the CDM.

N.7.4 Conjunction Data Message DCP Uncertainty and Sensitivity Vector Explanation

The content of Conjunction Data Message files produced by the United States Space Force's ASW software has been changed to enable conjunction risk assessments that account for covariance correlation. Specifically, ASW release versions 19.2 and after insert additional information within CDMs to enable users to include the atmospheric drag covariance cross-correlation effect when estimating a conjunction's probability of collision, as calculated from DCP uncertainty values and sensitivity vectors (as described in the previous section). This section provides an overview of these CDM modifications, and a brief description of their usage.

CDM Mean Position/Velocity State Vectors

CDMs can contain the mean position/velocity state vectors of the primary and secondary satellites at TCA in a couple of reference frames, as described in more detail in the CDM specification documents by Consultative Committee for Space Data Systems (specifically, CCSDS 502.0-B-1 and 502.0-B-2, listed in the references section). For Pc computation, an inertial reference frame must be used, sometimes requiring these original CDM states to be converted into the inertial reference frame. This section denotes the resulting mean inertial position and velocity vectors at TCA for the primary and secondary objects as $(\bar{\mathbf{r}}_p, \bar{\mathbf{v}}_p)$ and $(\bar{\mathbf{r}}_s, \bar{\mathbf{v}}_s)$, respectively.

[2] From Casali et al. 2018.

CDM Position/Velocity State Covariance Matrices

CDMs specify position/velocity state covariance matrices for the primary and secondary satellites using the radial-transverse-normal (RTN) coordinate frame. A CDM file specifies this symmetric 6×6 covariance for each object using keyword values for its 21 non-redundant matrix elements as follows

$$\boldsymbol{\mathcal{C}} = \begin{bmatrix} \mathcal{C}_{R,R} & \mathcal{C}_{T,R} & \mathcal{C}_{N,R} & \mathcal{C}_{\dot{R},R} & \mathcal{C}_{\dot{T},R} & \mathcal{C}_{\dot{N},R} \\ \mathcal{C}_{T,R} & \mathcal{C}_{T,T} & \mathcal{C}_{N,T} & \mathcal{C}_{\dot{R},T} & \mathcal{C}_{\dot{T},T} & \mathcal{C}_{\dot{N},T} \\ \mathcal{C}_{N,R} & \mathcal{C}_{N,T} & \mathcal{C}_{N,N} & \mathcal{C}_{\dot{R},N} & \mathcal{C}_{\dot{T},N} & \mathcal{C}_{\dot{N},N} \\ \mathcal{C}_{\dot{R},R} & \mathcal{C}_{\dot{R},T} & \mathcal{C}_{\dot{R},N} & \mathcal{C}_{\dot{R},\dot{R}} & \mathcal{C}_{\dot{T},\dot{R}} & \mathcal{C}_{\dot{N},\dot{R}} \\ \mathcal{C}_{\dot{T},R} & \mathcal{C}_{\dot{T},T} & \mathcal{C}_{\dot{T},N} & \mathcal{C}_{\dot{T},\dot{R}} & \mathcal{C}_{\dot{T},\dot{T}} & \mathcal{C}_{\dot{N},\dot{T}} \\ \mathcal{C}_{\dot{N},R} & \mathcal{C}_{\dot{N},T} & \mathcal{C}_{\dot{N},N} & \mathcal{C}_{\dot{N},\dot{R}} & \mathcal{C}_{\dot{N},\dot{T}} & \mathcal{C}_{\dot{N},\dot{N}} \end{bmatrix} \tag{N-11}$$

The RTN-frame covariance $\boldsymbol{\mathcal{C}}$ can be transformed into a 6×6 inertial frame position/velocity covariance $\mathbf{P}$ by applying the following equation

$$\mathbf{P} = \boldsymbol{\mathcal{M}}\, \boldsymbol{\mathcal{C}}\, \boldsymbol{\mathcal{M}}^T \tag{N-12}$$

with the 6×6 transformation matrix $\boldsymbol{\mathcal{M}}$ having the form

$$\boldsymbol{\mathcal{M}} = \begin{bmatrix} \mathbf{M} & \mathbf{0}_{3x3} \\ \mathbf{0}_{3x3} & \mathbf{M} \end{bmatrix} \tag{N-13}$$

with $\mathbf{0}_{3x3}$ representing a 3×3 matrix of zeros. The 3×3 orthonormal matrix $\mathbf{M}$ rotates vectors from the pseudo-inertial (non-rotating, instantaneously frozen) RTN frame into the inertial frame

$$\mathbf{M} = [\hat{\mathbf{R}}\ \hat{\mathbf{T}}\ \hat{\mathbf{N}}] \tag{N-14}$$

with column vectors given by the three RTN unit vectors, calculable from the object's inertial mean position and velocity vectors as follows

$$\hat{\mathbf{R}} = \bar{\mathbf{r}}/|\bar{\mathbf{r}}| \qquad \text{and} \qquad \hat{\mathbf{N}} = (\bar{\mathbf{r}} \times \bar{\mathbf{v}})/|\bar{\mathbf{r}} \times \bar{\mathbf{v}}| \qquad \text{and} \qquad \hat{\mathbf{T}} = \hat{\mathbf{N}} \times \hat{\mathbf{R}} \tag{N-15}$$

The 6×6 inertial frame covariance in eq. (N-12) can each be decomposed into three 3×3 sub-matrices

$$\mathbf{P} = \begin{bmatrix} \mathbf{A} & \mathbf{B}^T \\ \mathbf{B} & \mathbf{C} \end{bmatrix} \tag{N-16}$$

with $\mathbf{A}$ representing the marginalized covariance of the position vector, $\mathbf{C}$ the marginalized covariance of the velocity vector, and $\mathbf{B}$ position-velocity cross correlations.

Eqs. (N-11) to (N-16) can be used to calculate inertial frame position/velocity state covariance matrices at TCA for the primary and secondary objects involved in a conjunction, $\mathbf{P}_p$ and $\mathbf{P}_s$, respectively, as well as the marginalized position covariance matrices, $\mathbf{A}_p$ and $\mathbf{A}_s$. (Note: because RTN is an object-specific frame of reference, these calculations must employ different rotation matrices, $\mathbf{M}_p$ and $\mathbf{M}_s$, respectively.)

Uncorrelated and Correlated Relative Position Covariance Matrices

Collision probability estimation using the 2D-Pc method requires the conjunction's inertial relative position miss-vector, $\bar{\mathbf{r}}_m = \bar{\mathbf{r}}_s - \bar{\mathbf{r}}_p$, along with the associated miss-vector covariance matrix, $\mathbf{A}_m$. If the primary and secondary position vectors are statistically independent (i.e., uncorrelated), then the relative position miss-vector covariance is given by their sum

$$\mathbf{A}_m = \mathbf{A}_p + \mathbf{A}_s \tag{N-17}$$

This approach provides a viable approximation for 2D-Pc estimation for conjunctions in which $\mathbf{A}_p$ and $\mathbf{A}_s$ have sufficiently weak correlation. However, as described in the previous section, Casali et al. (2018) have demonstrated that some conjunctions have stronger covariance correlations, due to shared atmospheric density forecast components arising from the ASW global density portion of the Dynamic Consider Parameter. In these cases, the miss-vector covariance can be corrected by removing the cross-correlated components as follows

$$\mathbf{A}_m = \mathbf{A}_p + \mathbf{A}_s - \sigma_{p/g}\sigma_{s/g}\left[\mathbf{G}_p\mathbf{G}_s^T + \mathbf{G}_s\mathbf{G}_p^T\right] \tag{N-18}$$

with $\sigma_{p/g}$ and $\sigma_{s/g}$ denoting the atmospheric density 1-sigma relative uncertainties for the primary and secondary, respectively. The vectors $\mathbf{G}_s$ and $\mathbf{G}_p$ represent the sensitivity of the miss-vector covariance on global density relative uncertainties. (Note: see eq. (11) of Casali et al. (2018) and the related discussion for a derivation of eq. (N-18), and a more detailed explanation of its components. Also, this section uses the symbol "**A**" for 3×3 position covariances, instead of the symbol "**P**" which this section uses to represent full 6×6 position/velocity covariances. This change of notation means that eq. (N-18) is simply a restatement of eq. (N-10), the latter of which uses the original Casali et al. (2018) notation.)

CDM files produced by ASW versions 19.2 and later provide the sigma values and sensitivity vectors required to calculate corrected relative position covariance matrices using eq. (N-18). These data have been added within "comment" lines in the primary and secondary object portions of the CDM, with the format

COMMENT DCP Density Forecast Uncertainty=2.45030416E-01

COMMENT DCP Sensitivity Vector RTN Pos=-1.67441647E+01 3.68889831E+02 1.63797508E-01 [m]

COMMENT DCP Sensitivity Vector RTN Vel=-3.98670591E-01 1.09452965E-02 -4.83454839E-04 [m/sec]

The first occurrence of parameters with this specific format appears in the primary object section of the CDM and provides $\sigma_{p/g}$ (the DCP density forecast 1-sigma uncertainty), $\mathbf{G}_p^{RTN}$ (the 3×1 DCP position sensitivity vector, expressed in the primary's RTN frame), and $\mathbf{H}_p^{RTN}$ (the 3×1 DCP velocity RTN-frame sensitivity vector). The second occurrence provides the corresponding DCPs for the secondary, i.e., $\sigma_{s/g}$, $\mathbf{G}_s^{RTN}$ and $\mathbf{H}_s^{RTN}$. The RTN frame sensitivity vectors provided in the CDM can be converted to inertial frame vectors using the transformation matrix defined in eq. (N-14) separately for each object:

$$\mathbf{G}_p = \mathbf{M}_p\mathbf{G}_p^{RTN} \quad \text{and} \quad \mathbf{G}_s = \mathbf{M}_s\mathbf{G}_s^{RTN} \quad \text{and} \quad \mathbf{H}_p = \mathbf{M}_p\mathbf{H}_p^{RTN} \quad \text{and} \quad \boldsymbol{H}_s = \mathbf{M}_s\mathbf{H}_s^{RTN} \tag{N-19}$$

Uncorrelated and Correlated Relative Position/Velocity Covariance Matrices

For statistically independent primary and secondary states, the relative position/velocity miss-state covariance is given by the sum of the covariances for the two objects

$$\mathbf{P}_m = \mathbf{P}_p + \mathbf{P}_s \tag{N-20}$$

This approach provides a viable approximation for conjunctions in which the primary and secondary position/velocity states have sufficiently weak correlation. In other cases, the miss-vector covariance can be corrected by removing the cross-correlated components as follows

$$\mathbf{P}_m = \mathbf{P}_p + \mathbf{P}_s - \sigma_{p/g}\sigma_{s/g}\left[\mathbf{\Gamma}_p\mathbf{\Gamma}_s^T + \mathbf{\Gamma}_s\mathbf{\Gamma}_p^T\right] \tag{N-21}$$

with $\sigma_{p/g}$ and $\sigma_{s/g}$ again denoting the atmospheric density 1-sigma relative uncertainties for the primary and secondary objects, respectively. The 6×1 vector $\mathbf{\Gamma}_p = [\mathbf{G}_p^T\ \mathbf{H}_p^T]^T$ represents the sensitivity of the primary object's miss-state covariance on global density relative uncertainties. The secondary object's 6×1 sensitivity vector, $\mathbf{\Gamma}_s$, is defined similarly. (Again, see Casali et al. (2018) for more detail on these DCP uncertainties and sensitivity vectors.) The RTN frame sensitivity vectors provided in the CDM can be converted to inertial frame vectors using the transformation matrix defined in eq. (N-13) for each object

$$\mathbf{\Gamma}_p = \boldsymbol{\mathcal{M}}_p\mathbf{\Gamma}_p^{RTN} \qquad \text{and} \qquad \mathbf{\Gamma}_s = \boldsymbol{\mathcal{M}}_s\mathbf{\Gamma}_s^{RTN} \tag{N-22}$$

Pc Estimates with and without Covariance Correlation Correction

Conjunction 2D-Pc values calculated using the miss-vector covariance in eq. (N-18) represent collision probabilities corrected for global atmospheric cross-correlation effects. These can differ from the uncorrected 2D-Pc values calculated using the covariance in eq. (N-17). As shown in Figure N-11, analysis of archived conjunctions indicates that this correction usually does not change Pc values appreciably, except in a minority of conjunctions that have both elevated drag energy dissipation rates and an appropriate combination of orbital geometries. Among this minority, however, the corrections can potentially elevate Pc values by a factor of 1.5 or more (as shown on the right side of the plot in Figure N-11), meaning that accurate and conservative risk assessments for these cases rely on applying the covariance cross-correlation corrections made possible by the ASW system's recent CDM modifications.

For low-velocity or multi-conjunction interactions, the statistically expected number of collisions (i.e., the "3D-Nc" value) can be calculated using a miss-state covariance matrix of the same form as given in eq. (N-21), which then can be used to estimate the Pc value for the interaction, as explained in more detail by Hall (2021).

N.8 Monte Carlo Pc Calculation Techniques

Analytic approaches to Pc calculation are more computationally efficient than Monte Carlo methods, especially the conjunction plane two-dimensional Pc method. However, as discussed previously, analytic methods require certain enabling assumptions that are not necessarily valid for all conjunctions. Monte Carlo approaches require fewer enabling assumptions, but they are not typically employed as the first method of computation. Instead, Monte Carlo methods are usually reserved for cases that are suspected of violating the enabling assumptions of the analytic

methods. As described by Hall et al. (2018) and Hall (2021), there are two strains of the Monte Carlo method that are regularly employed:

- "Monte Carlo from epoch," in which the orbit-determination-epoch mean states and covariances are used to generate sampled states, and potentially long (i.e., multiday) high-fidelity propagations are required for each Monte Carlo trial.
- "Monte Carlo from TCA," in which the mean states and covariances predicted at TCA are used to generate sampled states, and only relatively short propagations to each trial's new TCA are required.

Each of these two approaches will be discussed in turn.

N.8.1 Monte Carlo from Epoch

The principal appeal of calculating the Pc using the Monte Carlo from epoch approach is that it requires almost no simplifying or restrictive assumptions, making it is as close to a "gold standard" for Pc estimation as can be devised. The input information includes the states and covariances for the primary and secondary objects at their respective orbit-determination epoch times, the combined hard-body radius of the two objects, and an ensemble of environmental datasets required for the high-fidelity propagations (such as predicted space weather indices and atmospheric density debiasing data; see Hall et al. 2018). The most elaborate instantiation of this technique uses the full eight-dimensional orbital state vectors (each containing six coordinate or element variables, plus drag and solar radiation pressure variables) along with the associated 8x8 covariance matrices for the primary and secondary satellites.

For each Monte Carlo trial, a state perturbation is obtained by performing a random draw from the distribution using the covariance matrix to generate the associated Gaussian distribution for each variable. These perturbations are then used to alter the initial states by adding each to the appropriate epoch mean state estimates. To do this for the primary satellite, for example, one would generate random perturbations for the eight variables representing the primary satellite's state based on their distribution as defined by the covariance, and then create a new, sampled state vector by adding the (signed) perturbations to the mean epoch state vector. This same procedure would also be performed for the secondary satellite. This sampling process generates epoch states for both the primary and secondary objects that represent statistically reasonable alternatives for their actual states. These two sampled epoch states are then propagated forward, a TCA identified, and a check performed to determine whether the miss distance at TCA is smaller than the hard-body radius; if it is, the trial results in a simulated collision and a "hit" is registered; if not, it is considered a "miss." This sampling/ propagation/ hit-registration procedure is then repeated for a large number of Monte Carlo trials, and the final number of hits divided by the total number of trials constitutes the Monte Carlo Pc estimate. There are algorithms that can be applied to estimate the confidence interval on the Monte Carlo Pc after a given number of trials due to event counting uncertainties (e.g., MATLAB's *binofit* function).

This procedure seems straightforward enough, and in many respects it is. But there are subtleties that require attention, especially if the technique is deployed for LEO conjunctions:

- For the result to be valid, the same force models and force model settings must be used for the Monte Carlo propagations as were used when generating the original orbit-determination solution. While it often is not difficult to apply the same general force model settings, there does need to be overall compatibility between the orbit-determination engine and the Monte Carlo propagator, such as the same set of geopotential Legendre polynomial coefficients (not just the same geopotential order) and, most critically for LEO, the same atmospheric density model. While it may be possible to deviate somewhat from this level of compatibility and still obtain reasonably accurate outcomes, the "gold standard" propriety of the result is lost.
- Correlation between the primary and secondary covariances, as described in the previous section, should be considered. This correlation can be modeled during the random draw process by forcing correlation in the primary and secondary objects' drag perturbations.
- Monte Carlo from epoch often requires extremely long computation run times. The run time is a function of the actual Pc, since this will determine how often hits are likely to occur and the number of trials required to obtain a result with a desired confidence level. Without marshalling extensive high-performance computing, the Pc levels that can be explored with this method have to remain relatively large (e.g., 10^{-5} or above). Computation times for smaller Pc events can be prohibitively long. For example, validating a Pc estimate of $\sim 10^{-7}$ at the 95% confidence level for a conjunction with TCA five days from the orbit determination epoch time would require an estimated two years of execution time on a 20-CPU, reasonably modern server (Hall et al. 2018). For this reason, it is typically necessary to reserve the Monte Carlo from epoch method for larger Pc events only, which means that one must trust analytic methods to identify a candidate subset of conjunctions for follow-up Monte Carlo analysis.
- High-fidelity orbital state propagations require the most processing during typical Monte Carlo from epoch computations, so when applying this approach, there is a temptation to "reuse" propagations to gain computational efficiency. Suppose that ten perturbations were performed for the primary satellite and ten propagated ephemerides were generated, and the same was done for the secondary object as well. Ephemeris #1 for the primary could be compared to ephemeris #1 for the secondary to determine whether a hit occurred, ephemeris #2 for the primary to ephemeris #2 for the secondary, ephemeris #3 for the primary to ephemeris #3 for the secondary, etc., and have as a result ten comparisons/trials. To go further, one could compare ephemeris #1 for the primary to ephemeris #2 for the secondary, ephemeris #1 for the primary to ephemeris #3 for the secondary, etc., and realize 100 comparisons/trials from merely 20 total propagations. Such a procedure certainty seems advantageous, given that processing time is the limiting factor to the deployment of Monte Carlo from epoch, and following such a procedure will produce a result that converges on the true Pc. The drawback is that such reuse of samples violates the conditions for the proper application of the formulae to calculate Pc uncertainty confidence intervals. Monte Carlo results without associated reliable confidence intervals are not operationally useful because it is never known how close one is to the true Pc value. Schilling et al. (2016) discuss this issue and confirm it to be a

problem, and they recommend some estimation techniques that allow (large) confidence intervals to be constructed around Monte Carlo products that avail themselves of sample reuse. The CARA implementation has avoided any such sample reuse to ensure that the "gold standard" status of the results not be in question and to produce more narrow confidence intervals.

Due to all the above considerations, but especially the run-time requirements, Monte Carlo from epoch is usually reserved only for those cases that require it for accurate Pc estimation.

A study effort discussed in greater detail in the next section determined that the Monte Carlo from epoch method appears to be needed only when the two objects stay in such close proximity that they experience a sequence of multiple, comparable-risk close approaches during a multiday risk assessment projection interval. For closely spaced co-orbiting objects, these conjunctions may also become effectively "blended" in time with one another such that collision probability accumulates appreciably even during the mid-point times between the encounters rather than just during short bursts very near the close approaches (Baars et al. 2019). In such cases, two impediments arise to estimating accurate Pc values using methods formulated for temporally isolated close approaches. First, there is no clear, single TCA at which to evaluate the collision likelihood. While one could in fact find the unique point of closest approach between the two nominal trajectories for the entire sequence and perform a two-dimensional Pc calculation for that encounter, there is no guarantee that another encounter in the sequence may actually possess a higher Pc due to different covariance orientations even though it has a larger nominal miss distance. Second, calculating a single encounter Pc at each of the close approaches and then amalgamating these using the following formula (derived from DeMorgan's Law of Complements)

$$P_{Tot} = 1 - \prod_{i=1}^{n}(1 - P_{ci}) \qquad \text{(N-23)}$$

potentially overestimates the overall collision likelihood because it presumes that the individual events in the sequence are statistically independent, but in fact they may not be, especially if blended in time. This total probability estimate matches that given in equation (N-8) and provides an upper bound for the amalgamated risk over the time interval of interest. For maximum efficiency, Monte Carlo from epoch would then be run operationally only in cases in which this upper bound is above a mitigation threshold and there is interest in determining whether the higher-fidelity Monte Carlo calculation would reduce this value to one much closer to or below the threshold. Monte Carlo from epoch can also be run if there is any question about the overall rectitude of the Pc calculation. As stated earlier, lower-Pc conjunctions may present intractable Monte Carlo execution times, but if one wishes only to ensure that the Monte Carlo Pc falls below the mitigation threshold (rather than establish a high-fidelity Pc value), this can usually be accomplished with far fewer Monte Carlo trials.

Optimal application of the Monte Carlo from epoch Pc estimation method does not entail Pc evaluation over a relatively short time interval bracketing a single conjunction's TCA, but rather over a more extended interval that spans several close approach encounters. For example, the collision likelihood between two objects would not be evaluated at the nominal TCA for a single conjunction, but, perhaps, over a risk assessment interval projecting forward seven days. This

multiday interval would not only include the original nominal TCA but also a sequence of other encounters between the primary and secondary as well. In this case, each Monte Carlo trial would be propagated forward seven days and a hit registered at the earliest time that the hard-body radius is violated, if such a time exists (Hall et al. 2018 and Hall 2021). Temporal risk plots can be produced using the sequence of hits registered during all the trials, an example of which is shown in Figure N-12 (which shows the same conjunction sequence as Figure N-8 from the earlier discussion of two- and three-dimensional Nc calculation methods). The pink shaded area in Figure N-12 shows the Monte Carlo Pc estimation confidence region, and the pink line shows the best estimate Monte Carlo result. As can be seen, the black upper line, which is the upper bound estimate from the three-dimensional Nc function, is within the confidence interval of the Monte Carlo results and thus is a reasonable actual realization of the repeating conjunctions' cumulative risk.

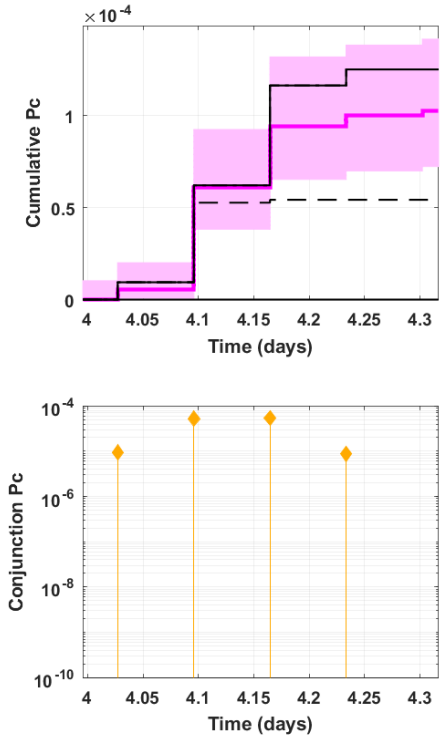

Figure N-12 Three-Dimensional Nc Temporal Risk Plot with Monte Carlo from Epoch Result Overlay (in Pink)

Because it is complicated to set up the execution environment for the Monte Carlo from epoch calculation, and because "gold standard" results require assembling extensive environmental data and software settings identical to the original DOD orbit-determination solutions, it is envisioned that the ability to run this strain of Monte Carlo estimation will remain with NASA CARA. However, a more computationally efficient mode of Monte Carlo estimation, which is serviceable for several different applications and is easier to obtain and employ operationally, is described in the next section.

N.8.2 Monte Carlo from TCA

A much more computationally efficient variant on Monte Carlo from epoch, which has been used by conjunction assessment practitioners for some time, is Monte Carlo conducted from TCA, or two-body Monte Carlo (TBMC)-Pc estimation. As the definition implies, the Monte Carlo simulation begins with the primary and secondary objects' equinoctial element states propagated to TCA. Perturbation and sampling of both states is conducted much as described earlier for Monte Carlo from epoch, and each sampled primary and secondary state is propagated both forward and backward in time to find the pair's TCA and determine whether the corresponding miss distance is smaller than the hard-body radius (backward propagations are required to register hits that occur at times before TCA). The simplification arises from the fact that, since one is beginning from TCA, the propagations required will be short. This means that an efficient two-body motion propagation scheme usually provides an accurate trajectory approximation, and this, combined with the very short propagation times, vastly improves the computational efficiency of the calculation—by a factor of 10,000 to 100,000 according to the study by Hall et al. (2018). This specific method of Monte Carlo from TCA is also referred to as "two-body Monte Carlo" Pc (TBMC-Pc) estimation. To use the TBMC-Pc method, the conjunction duration needs to be short so that one may safely presume a single, unblended event that does not require the Monte Carlo from epoch method. As a second condition, one must have confidence that both objects' states and covariances propagated to TCA are good representations of the states and state uncertainties at that point. Usually, there is reasonable confidence in the mean state estimates themselves, but the covariances are a different matter: a number of studies (e.g., DeMars et al. 2014) have indicated that propagated covariances represented in Cartesian space fail to represent the actual uncertainty distributions, due both to the potential failure of the linearized dynamics to remain representative over long propagation intervals and, more importantly, a mismatch between elongated in-track uncertainty volumes and the forced representation of these uncertainty volumes as Cartesian ellipsoids. The latter problem is illustrated in Figure N-13. The actual in-track error volume should follow the curved trajectory of the orbit, but the Cartesian covariance is limited to the rectilinear representation shown: as the elongation grows in the in-track direction (which occurs for longer propagations), the mismatch between the two representations also increases.

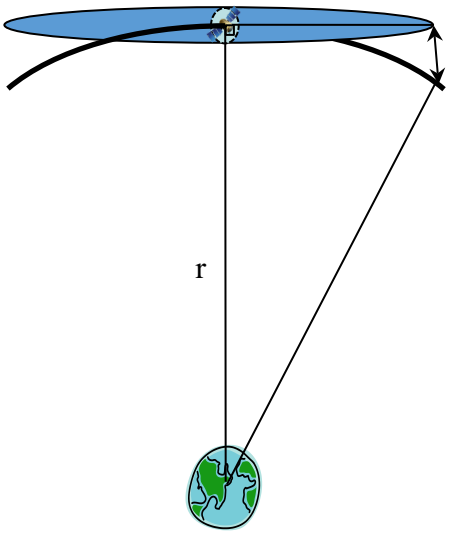

Figure N-13 Mismatch between Elongated In-track Covariances and Forced Cartesian Ellipsoidal Representation

To address the latter problem, the results from a study conducted by Sabol et al. (2010) are both important and extremely helpful. This study addressed directly the question of the optimal choice of orbital state representation for covariances, finding that it is not the specific state representation in which the propagation is executed but rather the one in which the propagated covariance is rendered that ultimately governs the realism of the uncertainty distribution and associated error volume. Specifically, if the covariance is rendered and used in a curvilinear state representation, such as equinoctial elements, then it tends to represent the error volume much more accurately than if it is transformed and used in Cartesian coordinates. The surprising result is that a non-representative Cartesian covariance transformed into an equinoctial covariance becomes a representative covariance. Furthermore, taking random samples using the equinoctial state representation and performing the non-linear conversion of each sample to Cartesian coordinates generates a point cloud in the Cartesian frame that also approximates the true error volume much more accurately.

This latter procedure allows the Monte Carlo from TCA method to employ more realistic uncertainty volumes, at least with respect to orbital state representation-related mismatches. The detailed procedure is the following:

1. Convert both objects' states and covariances at TCA to equinoctial elements.
2. Generate a set of perturbations for each object based on the equinoctial covariances.
3. Combine these with the mean equinoctial states to generate sampled equinoctial states for the primary and secondary.
4. Convert these sampled states from equinoctial elements to Cartesian coordinates using the non-linear transformation.

5. Propagate the Cartesian states for both the primary and secondary using two-body equations of motion to find the new TCA, which may precede or follow the nominal TCA.
6. Determine whether the new miss distance is less than the hard-body radius, and if so, register a hit at the time that the hard-body radius sphere is violated.
7. Repeat steps 5-6 until the entire set of Monte Carlo sampling trials has been processed.
8. The Pc is the number of hits divided by the total number of trials, and the confidence interval can be calculated from an appropriate formula.

This approach seems reasonable enough; but it would be presumptuous to assert, without further study, that it is truly robust, especially since the question of the durability of the linearized dynamics typically used to propagate covariances was not directly addressed. As it is, additional study efforts have been performed to verify that it is indeed sufficiently representative for conjunction assessment applications, and they are described below.

The first of these study efforts was performed as part of the previously cited analysis by Hall et al. (2018). A set of 373 high-Pc conjunctions was selected and evaluated with both Monte Carlo from epoch and Monte Carlo from TCA, and the comparative results are shown in Figure N-14. The top window is a scatter plot of the Pc calculated by Monte Carlo from epoch versus that from Monte Carlo from TCA. The intersection of each "plus" sign gives the scatter-plot point, and the length of the plus-symbol tails indicates the uncertainty of the calculation. One can see that the agreement is strong because all the points are close to the dashed y-x line that would indicate perfect equality. The bottom window plots the base-ten logarithm of the ratio of Pc values estimated using the Monte Carlo from epoch method to those estimated with the Monte Carlo from TCA method. The largest deviations are about 0.2 of an order of magnitude in Pc, which is considered to be below operational significance. A separate statistical test for similarity of results produced *p*-values all less than 10^{-3}, indicating that one should reject a hypothesis that these results arise from different distributions. Good agreement is thus observed between the abbreviated Monte Carlo from TCA and Monte Carlo from epoch results.

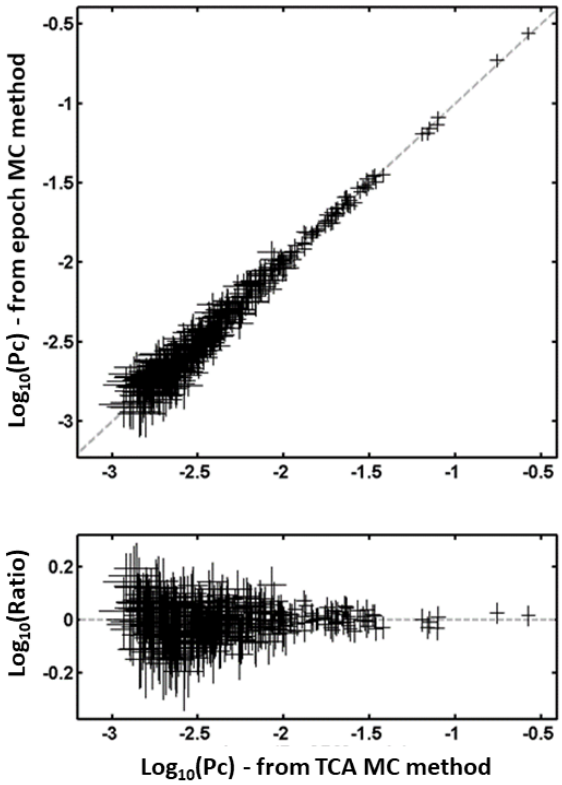

Figure N-14 Comparative Results of 373 High-Pc Conjunctions[3]

The second study effort involved a comparison between the Monte Carlo from TCA Pc estimation method and the two-dimensional Pc method (Hall 2019b), which was later extended to compare the from TCA method to two- and three-dimensional Nc methods (Hall 2021). In these studies, 63,603 temporally isolated conjunction events with two-dimensional Pc values greater than 10^{-7} were subjected to Pc calculation by the two-dimensional Pc method, as well as the two- and three-dimensional Nc methods, and all of these were compared to the Monte Carlo from TCA method. The comparative results are shown in Figure N-15 (which refers to Pc values estimated using the Monte Carlo from TCA method as TBMC-Pc values). These plots are similar to those already shown in Figure N-7, except in this case the colored diamonds represent the worst kind of Pc estimation failure, i.e., conjunctions in which the analytical calculations significantly underestimate the Monte Carlo from TCA method Pc values. The left panel shows that, although the two-dimensional Pc method performs reasonably well for the vast majority of temporally isolated conjunctions, it underestimates from TCA Pc values by a factor of 1.5 or more in 0.258% of the investigated cases. (See the top legend of the left graph.) For those cases that showed large disparities, the subset that had true Pc values in the tractable range for Monte Carlo from epoch were validated with this methodology; and in each case the Monte Carlo from epoch reruns matched the output from the Monte Carlo from TCA. To the degree that non-representative covariances may be responsible for two-dimensional Pc failures (due to coordinate frame mismatches), Monte Carlo from TCA certainly appears to be able to recover the true Pc.

[3] From Hall et al. 2018.

As an aside, some of these differences between the conjunction plane two-dimensional Pc estimates and the Monte Carlo method estimates are considerable; there are several cases in which the two-dimensional Pc estimate understates the Monte Carlo from TCA estimate by more than an order of magnitude, as shown in the red in the left panel of Figure N-15. The center and left panels of Figure N-15 show that the three- and two-dimensional Nc methods do not similarly underestimate the from TCA Pc method values, except in a few statistically insignificant cases.

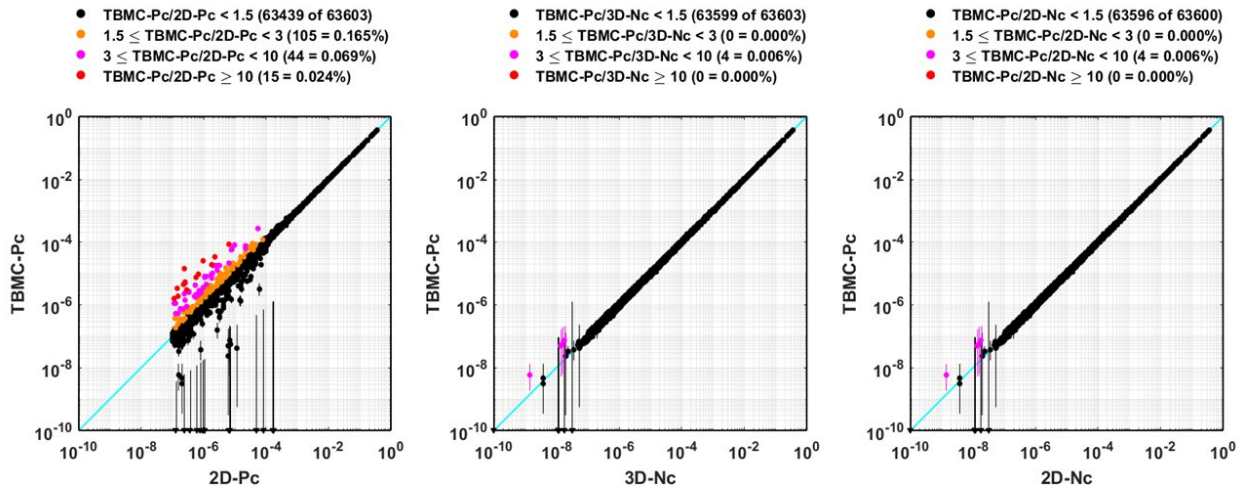

Figure N-15 Comparative Results of 63,603 Conjunction Events[4]

Originally, Monte Carlo from TCA was advanced as a robust and computationally tractable way to ensure reliable Pc calculations in the face of occasional miscarriage of the two-dimensional Pc algorithm. However, Figure N-15 demonstrates that the development and testing of the two- and three-dimensional Nc analytic methods have led NASA CARA to recommend that these methods supplant routine use of Monte Carlo from TCA. One may still resort to this more computationally efficient Monte Carlo method if desired, but testing indicates that the Nc calculation methods outperform Monte Carlo from TCA (in that it accurately matches Pc estimates for isolated conjunctions and also provides a cumulative risk upper bound for repeating conjunctions) and is at least an order of magnitude more computationally efficient, especially for events with small Pc values. Monte Carlo from TCA is a capability available for download from the NASA CARA software repository,[5] and O/Os who are currently using it or a similar implementation are not urged to take it out of service, but as a Pc calculation approach, it does not seem to offer any enduring advantage over the two- and three-dimensional Nc methods.

Finally, a dedicated study on covariance Gaussianity was recently conducted (Lechtenberg 2019b). The same set of 44,000 conjunctions used by Hall (2019b) was analyzed for multivariate normality of the position covariance in Cartesian coordinates. The methodology was to convert the covariance to equinoctial elements, generate a set of random position samples from this covariance, convert the sample set to Cartesian coordinates, and apply a multivariate normality

[4] From Hall 2019b and Hall 2021.
[5] Specifically, the *MCWorkbench* SDK function estimates TBMC-Pc conjunction values using CDM test files as input. See Section 7, Contact Information in this document for the CARA software repository URL.

test (here the Henze-Zirkler test) to assess compliance to this distribution. At a 5% significance level, only 60% of the cases could be considered to conform to a multivariate Gaussian distribution in Cartesian coordinates. In principle, such conjunctions would be considered suspect cases whose two-dimensional Pc results would be considered doubtful. As it is, since such a large fraction of the investigated cases show good agreement between the Monte Carlo at TCA and the two-dimensional Pc, clearly the Gaussianity of the covariances in the Cartesian framework does not matter appreciably for the Pc calculation. This result corroborates that of an earlier study by Ghrist and Plakalovic (2012), which reported similar findings.

How can this be, given that the covariance is integral to the two-dimensional Pc calculation? It is important to remember that the analyses above are restricted to high-Pc events. For the probability of collision to be high, significant overlap needs to exist between the primary and secondary object covariances; this means that the central parts of the covariances, which are where most of the probability density lies, have to overlap substantially. Such a requirement makes the behavior of the tails of the covariance much less important, and it is in the tails that non-Gaussian behavior is most strongly manifested. Even though a good number of conjunctions fail tests for covariance Gaussianity in Cartesian coordinates, for high-Pc events, this result does not appear to affect the rectitude of the calculated Pc. A difference probably is observable for lower-Pc conjunctions, but because these conjunctions are not operationally significant, it is not operationally important to identify or characterize this phenomenon.

There is the lingering question of the eventual failure of the linearized dynamics in propagating covariances since DOD covariances are propagated through a pre- and post-multiplication by a linearized state transition matrix. It is agreed that, given sufficiently long propagations, such an eventuality should arise. However, the propagation duration required for this problem to manifest itself substantially is believed to be much longer than encountered for most conjunctions—on the order of weeks. This is why more attention is paid to this phenomenon in other areas of SSA such as uncorrelated track processing for which propagations of 30 days or more may be required, whereas it is rare for propagations longer than ten days to take place in conjunction assessment. Of course, fresh tracking data are always appreciated as they shorten the propagation interval and lend additional confidence to the solution.

N.9 Choosing an Appropriate Hard-Body Radius

As discussed in the first section of this appendix, the hard-body radius represents the combined size of the primary and secondary objects; the word “radius” is used because this combined size is typically envisioned as a sphere, and the radius of a sphere is a convenient linear representation of its size. The hard-body radius is needed for the Pc calculation because it represents the circle/sphere within which a simultaneous penetration by both the primary and secondary objects’ trajectories will constitute a presumed collision. It is not just a required input to the Pc calculation, however, it is also one of the governing parameters of the calculation: the Pc value represents an integral over the area of the hard-body radius circle (or surface area of the hard-body radius sphere) and thus in many circumstances, varies roughly in proportion to the square of the hard-body radius, so an increase of the hard-body radius by a factor of three increases the calculated Pc by a factor of nine, or nearly one order of magnitude. Because of this sensitivity, it is important not to overstate the hard-body radius simply for “conservatism”

because the effect on the calculated Pc can be considerable. The best overall strategy for applying conservatism, should one wish that, is to apply it at the end of the process by lowering the Pc threshold at which mitigation actions should occur. Injecting conservatism into different places throughout the Pc calculation makes it difficult to determine how much conservatism has actually been introduced, whereas addressing this desire through a modification of the Pc threshold for mitigation allows it to be understood precisely.

Mashiku and Hejduk (2019) recently completed a study of different hard-body radius calculation and setting strategies, and a streamlined summary of the possibilities examined is provided below:

1. **Large *a priori* value**. For some years it was standard practice simply to choose a hard-body radius value that was notably larger than the expected actual size of the combined primary and secondary object; 20 meters is a value that was typically used. Perhaps in the early days of conjunction assessment, this was an acceptable initial screening strategy to identify potential serious events, and the hard-body radius would then be reduced when analysis began in earnest. As the space catalog has grown in size, and especially with the recent growth through the deployment of the Space Fence radar, this particular strategy merely creates additional false alarms that needlessly burden the process. Nearly all O/Os have moved away from this hard-body radius strategy.
2. **Circumscribing sphere**. The use of a circumscribing sphere to set the primary object's hard-body radius is perhaps the most commonly used present operational technique, which admits of two typical variants: placing the sphere's center at the center of mass of the primary satellite and defining the radius by the length from this center to the satellite's most distant extremity; or allowing the center point to float freely and then defining the smallest circumscribing sphere. The overall sphere size then has to be increased by the expected size of the secondary object using either an averaged value or an estimate for the particular secondary encountered. This size could be obtained either from known or published dimensions (for intact spacecraft or rocket bodies) or estimated from remote sensing data, such as radar cross-section or photometric brightness measurements. In the latter case, the estimated hard-body radius size of the secondary may also have an associated uncertainty estimate, which can also be incorporated into the Pc estimation process (as discussed in more detail below).
3. **Maximum projected area into any plane**. Since the circumscribing sphere described above most often ends up being projected into the conjunction plane, it is instructive to examine in more detail the implications of such a projection. Clearly the sphere itself will project as a circle, but the projection of the three-dimensional spacecraft inside will necessarily be smaller in area than the projected circle, and for some spacecraft shapes and orientations, it will be substantially smaller in area. In this latter case, the substantial "white space" within the projected circular area not occupied by the primary could justifiably be excluded in the Pc estimation process, especially for the most common debris-encounter scenario when the incoming secondary object is much smaller than the primary asset. A straightforward way to address this issue that does require knowledge of the satellite's actual orientation in relation to the conjunction plane is simply to

determine in advance the maximum area that the satellite can possibly project into any plane (based on a three-dimensional CAD[6] model of the satellite) and use a hard-body radius circle of that equivalent area (which of course must then be enlarged to include the estimated size of the secondary) for Pc estimation. It is true that this is a conservative formulation in that it uses the maximum possible projected area, but this is often substantially smaller than the area of the projected circumscribing sphere. One could argue that uncertainty is introduced by using the equivalent circular area rather than a contour integral to perform the integration over the actual projected shape, but individual exploratory examples show that this difference is usually negligibly small, and in any case, the most conservative projection approach should compensate for any differences in the shape chosen to represent the hard-body radius area for the Pc calculation.

4. **Projection into actual conjunction plane**. The most accurate, and at the same time the most difficult, approach is to perform a projection of the primary satellite's shape into the actual conjunction plane. Specifically, this requires a three-dimensional CAD model of the satellite plus knowledge of its inertial attitude and the orientation of any major articulating components at TCA along with a calculation to project the resulting shape into the conjunction plane. Once this projection is obtained, its boundaries have to be augmented to account for the expected size of the secondary, and the integration of the joint covariance probability density can take place over this figure via contour integration or over a more convenient shape of equivalent area. Chan (2019) recently proposed a method to decompose complex shapes into individual triangles and use an equivalent-area method to evaluate the Pc for each triangle; the composite Pc is simply the sum of the Pc values for these individual trials of decomposition.

Each successive approach among the four presented brings greater precision to the hard-body radius determination but at the same time, additional complexity. A reasonable *via media* would appear to be approach 3) above, which keeps the hard-body radius value grounded in reality and free from excessive conservatism but avoids the difficulties of gathering and maintaining shape and attitude data to enable a detailed projection calculation for each conjunction.

To facilitate Pc estimation, CARA has undertaken an effort to estimate hard-body radii of unknown orbiting objects based on radar cross section (RCS) measurements obtained by the Space Fence radar system (Baars and Hall 2022; Hall and Baars 2022). Even after accounting for radar calibration irregularities and occasional outlier data points, such RCS measurements have considerable point-to-point scatter, and the process of converting the RCS data into hard-body radius estimates introduces considerable additional uncertainty. The resulting hard-body radius uncertainty PDFs are non-Gaussian, although they can be roughly approximated using a log-normal distribution. Notably, RCS-based hard-body radius estimates are typically uncertain by factors of two to three, so it is essential that Pc estimates account for these uncertainties. For an unknown secondary involved in a conjunction, the RCS-based uncertainty PDF can be used to calculate a mean hard-body radius estimate, $\bar{R}_2$, and an associated variance, $\sigma_{R_2}^2$. As mentioned previously, for many conjunctions, the estimated Pc value varies roughly in proportion to the

[6] Computer-aided Design

square of the hard-body radius. In these cases, the appropriate hard-body radius to use for Pc estimation is given by the effective combined hard-body radius

$$R_{\text{eff}} = \sqrt{(R_1 + \bar{R}_2)^2 + \sigma_{R_2}^2} \tag{N-24}$$

with R_1 representing the primary object's hard-body radius, usually established using methods 2 or 3 listed above. (The current recommendation for the less often used method 4 is to increase the projected shape of the primary object outwardly on the conjunction plane by the length $\bar{R}_2 + 3\sigma_{R_2}$ to produce a conservative Pc estimate, although CARA continues to research a more accurate approach in these cases.) So for most cases, CARA recommends calculating Pc values using the combined hard-body radius given in equation (N-24) for all conjunctions involving secondary objects with uncertain sizes, partly because of the formula's relative simplicity, but primarily because using the effective radius approach reproduces reasonably well the more accurate RCS-based Pc estimates calculated using Monte Carlo analyses. (See Hall and Baars 2022 for details.)

Currently, Space Fence RCS measurements sufficient for size estimation are available for over 90% of CARA conjunctions involving unknown secondary objects (Baars and Hall 2022). Analysis indicates that about 98% of such conjunctions involve secondary objects with mean hard-body radius estimates less than 35 cm, and only about 0.3% have $\bar{R}_2 > 1.5$ m. CARA uses a multi-faceted approach to estimate secondary sizes. For known secondary objects (e.g., active or retired payloads, rocket-bodies), the approach uses the known hard-body radii with zero uncertainty, tabulated along with a reference for the source of the size information. For unknown objects with sufficient RCS data (which includes a large fraction of tracked LEO orbital debris objects), the CARA approach tabulates the mean estimated hard-body radius and the 1-sigma uncertainty, which can be used in equation (N-24). For reference, this approach also tabulates the median hard body radius values, as well as the associated 95% and 99% confidence intervals, as estimated from the actual RCS-based uncertainty PDF. For unknown objects with insufficient RCS data, one can assign a reasonably conservative default size estimate of 1.5 m.

Authored and Other References

1. Abramowitz, M. and Stegun, I. A. 1970, *Handbook of Mathematical Functions*, New York, NY: Dover Publications, Inc.
2. Akella, M. R. and K. T. Alfriend. 2000. "The Probability of Collision Between Space Objects." *Journal of Guidance, Control and Dynamics*, Vol. 23 No. 5 (September-October 2000) pp. 769-772.
3. Alfano, S. 2004. "Orbital Covariance Interpolation." 14th AAS/AIAA Space Flight Mechanics Conference, Maui HI, February 2004.
4. Alfano, S. 2005a. "A Numerical Implementation of Spherical Object Collision Probability." *Journal of the Astronautical Sciences*, Vol. 53 No. 1 (January-March 2005), pp. 103-109.
5. Alfano, S. 2005b. "Relating Position Uncertainty to Maximum Conjunction Probability." *Journal of the Astronautical Sciences*, Vol. 53 No. 2 (April-June 2005), pp. 193-205.
6. Baars, L., Hall D., and Casali, S. 2019. "Assessing GEO and LEO Repeating Conjunctions using High-Fidelity Brute Force Monte Carlo Simulations." 2019 AAS Astrodynamics Specialist Conference (Paper #19-612), Portland ME, August 2019.
7. Baars, L. and Hall, D. 2022 "Processing Space Fence Radar Cross-Section Data to Produce Size and Mass Estimates" 2022 AAS Astrodynamics Specialist Conference (Paper #22-586), Charlotte, N.C., August 2022.
8. Balch, M. S., R. Martin, and S. Ferson. 2019. "Satellite Conjunction Assessment and the False Confidence Theorem." *Proceedings of the Royal Society A: Mathematical, Physical and Engineering Sciences*, Vol. 475, Issue 2227, 2019. (https://doi.org/10.1098/rspa.2018.0565).
9. Butt, Y. et al. 2021. See above: National Geospatial-Intelligence Agency (NGA), Cis-Lunar SSA Technical Steering Group. "Proposed Message Set For All Altitude Regimes." (DRAFT). November 2021. https://www.nasa.gov/sites/default/files/atoms/files/cislunar_ssa_proposed_message_set-nov2021_rev2_without_emailspdf.pdf
10. Bassa, C. G., Hainaut, O. R., and Galadi-Enriquezz, D. 2022. "Analytical Simulations of the Effect of Satellite Constellations on Optical and Near-infrared Observations." *Astronomy & Astrophysics* Vol. 657, P. A75, Jan 2022.
11. Carpenter, J. R. and F. L. Markey. 2014. "Wald Sequential Probability Ratio Test for Space Object Conjunction Assessment." *Journal of Guidance, Control, and Dynamics* Vol. 37 No. 5 (September-October 2014), pp. 1385-1396.
12. Carpenter 2019.
13. Carpenter 2020.

14. Casali, S., D. Hall, D. Snow, M. Hejduk, L. Johnson, B. Skrehart, and L. Baars. 2018. “Effect of Cross-Correlation of Orbital Error on Probability of Collision Determination.” 2018 AAS/AIAA Astrodynamics Specialist Conference (Paper #18-272), Snowbird UT, August 2018.

15. Consultative Committee for Space Data Systems (CCSDS) 508.0-B-1. Conjunction Data Message (CDM) Blue Book. Issue 1. Recommended Standard for Conjunction Data Messages. Washington, D.C.: CCSDS, June 2013. https://public.ccsds.org/Pubs/508x0b1e2c2.pdf.

16. CCSDS 502.0-B-2. Orbit Data Messages Blue Book. Issue 2. Recommendation for Space Data System Standards[7]. Washington, D.C.: CCSDS, November 2009. https://public.ccsds.org/Pubs/502x0b2c1e2.pdf.

17. Chan, F. C. 2008. *Spacecraft Collision Probability*. El Segundo, CA: The Aerospace Press.

18. Chan, F. C. 2015. “Formulation of Collision Probability with Time-Dependent Probability Distribution Functions,” AAS/AIAA Space Flight Mechanics Meeting (Paper #15-233), Williamsburg, VA, January 2015.

19. Chan, F. C. 2019. “Collision Probability for Polygonal Cross Sections.” 2019 AAS Astrodynamics Specialist Conference (Paper #19-911), Portland ME, August 2019.

20. Clopper, C. and E. S. Pearson. 1934. “The Use of Confidence or Fiducial Limits Illustrated in the Case of the Binomial.” *Biometrika*, Vol. 26 (1934), pp 404-413.

21. Coppola, V.T. 2012. “Including Velocity Uncertainty in the Probability of Collision between Space Objects.” AAS/AIAA Spaceflight Mechanics Meeting, Charleston SC, Paper 12-247, February 2012.

22. D’Agostino, R. B. and M. A. Stephens. 1986. *Goodness-of-Fit Techniques*. New York: Marcel Dekker, Inc.

23. DeMars, K., Y. Cheng, and M. Jah. 2014. “Collision Probability with Gaussian Mixture Orbit Uncertainty.” *Journal of Guidance, Control, and Dynamics*, Vol. 37 No. 3 (2014), pp. 979-985.

24. Elkantassi and Davison 2022.

25. Elrod, C. 2019. “Computational Bayesian Methods Applied to Complex Problems in Bio and Astro Statistics.” Doctoral Dissertation, Baylor University, July 2019.

26. Flohrer, T., Lemmens, S., Bastida Virgili, B., Krag, H., Klinkrad, H., Parrilla, E., Sanchez, N., Oliveira, J., Pina, F. 2013. “DISCOS – Current Status and Future Developments.” Proc. 6th European Conference on Space Debris, (ESA SP-723), Darmstadt, Germany, April 2013.

27. Folta, David, Natasha Bosanac, Ian Elliott, Laurie Mann, Rebecca Mesarch, and Jose Rosales. 2002. See above: NASA Technical Publication NASA/TP–20220014814,

[7] There is a version 3 Orbit Data Messages (ODM) that will be published relatively soon (early 2023), but it doesn't change the Orbit Ephemeris Message (OEM) in a material way.

"Astrodynamics Convention and Modeling Reference for Lunar, Cislunar, and Libration Point Orbits." 1 December 2022.

28. Foster, J. L., and H. S. Estes. 1992. "A Parametric Analysis of Orbital Debris Collision Probability and Maneuver Rate for Space Vehicles." NASA/JSC-25898 (August 1992).
29. Frisbee, J. 2015. "An Upper Bound on High-Speed Satellite Collision Probability when only One Object has Position Uncertainty Information." 2015 AAS/AIAA Astrodynamics Specialist Conference (Paper #15-717), Vail CO, August 2015.
30. Garcia-Pelayo, R. and Hernando-Ayuso, J. 2016. "Series for the Collision Probability in Short-Encounter Model," *Journal of Guidance Control and Dynamics*, Vol. 39, No. 8, pp. 1904-1912, Aug. 2016.
31. Ghrist, R. W., and D. Plakalovic. 2012. "Impact of Non-Gaussian Error Volumes on Conjunction Assessment Risk Analysis." 2012 AIAA/AAS Astrodynamics Specialist Conference, Minneapolis MN, August 2012.
32. Grubbs, F.E. 1969. "Procedures for detecting Outlying Observations in Samples." *Technometrics* 11 (1969), 1-21.
33. Hall, D.T., M. D. Hejduk, and L. C. Johnson. 2017a. "Time Dependence of Collision Probabilities During Satellite Conjunctions." AAS Space Flight Mechanics Meeting (Paper # 17-271), San Antonio, TX, February 5-9, 2017.
34. Hall, D.T., M. D. Hejduk, and L. C. Johnson. 2017b. "Remediating Non-Positive-Definite State Covariances for Collision Probability Estimation." 2017 AAS/AIAA Astrodynamics Specialist Conference, Stevenson WA, August 2017.
35. Hall, D.T., S. J. Casali, L. C. Johnson, B. B. Skrehart, and L. G. Baars. 2018. "High-Fidelity Collision Probabilities Estimated using Brute Force Monte Carlo Simulations." 2018 AAS/AIAA Astrodynamics Specialist Conference (Paper #18-244), Snowbird UT, August 2018.
36. Hall, D.T. 2019a. "Determining Appropriate Risk Remediation Thresholds from Empirical Conjunction Data using Survival Probability Methods." 2019 AAS Astrodynamics Specialist Conference (Paper #19-631), Portland ME, August 2019.
37. Hall, D.T. 2019b. "Implementation Recommendations and Usage Boundaries for the Two-Dimensional Probability of Collision Calculation." 2019 AAS Astrodynamics Specialist Conference (Paper #19-632), Portland ME, August 2019.
38. Hall, D.T. and Matney, M.M. 2000. "Collision Probabilities for Keplerian Orbits." Space Debris, Vol. 2. (2000), pp.161-198.
39. Hall, D.T. 2021. "Expected Collision Rates for Tracked Satellites," *Journal of Spacecraft and Rockets*, Vol. 58 No. 3 (2021), pp. 715-728.
40. Hall, D.T. 2022. "Semi-Empirical Astronomical Light Pollution Evaluation of Satellite Constellations." *Journal of the Astronautical Sciences*, .69, pp.1893-1928, 2022. doi.org/10.1007/s40295-022-00358-4.

41. Hall, D. and Baars, L. 2022, “Collision and Fragmentation Probabilities for Satellites with Size and Mass Estimates Based on Radar Observations.” In preparation, Nov. 2022.

42. Hall, D. T, Baars, L. B., and Casali, S. J. 2023 “A Multistep Probability of Collision Computational Algorithm.” 2023 AAS/AIAA Astrodynamics Specialist Conference (Paper #23-398), Big Sky MT, August 2023.

43. Hametz, M. E. and B. A. Beaver. 2013. “A Geometric Analysis to Protect Manned Assets from Newly Launched Objects – COLA Gap Analysis.” AAS 13-360.

44. Hejduk, M.D. 2008. “Space Catalogue Accuracy Modeling Simplifications.” 2008 AAS Astrodynamics Specialists Conference, Honolulu, HI, August 2008.

45. Hejduk, M.D., S. J. Casali, D. A. Cappellucci, N. L. Ericson, and D. E. Snow. 2013. “A Catalogue-Wide Implementation of General Perturbations Orbit Determination Extrapolated from Higher-Order Theory Solutions.” 2013 AAS/AIAA Space Flight Mechanics Meeting, Kauai, HI. February 2013.

46. Hejduk, M.D., D. Plakalovic, M. E. Hametz, L. K. Newman, J. C. Ollivierre, B. A. Beaver, and R. C. Thompson. 2014. “Launch COLA Operations: An Examination of Data Products, Procedures, and Thresholds, Revision A.” NASA Special Technical Report. 12 January 2014.

47. Hejduk, M.D., L. K. Newman, R. L. Besser, and D. A. Pachura. 2015. “Predicting Space Weather Effects on Close Approach Events.” 2015 AMOS Technical Conference, Kihei HI, September 2015.

48. Hejduk, M.D., F. Laporte, M. Moury, T. S. Kelso, L. K. Newman, and R. Shepperd. 2017. “Consideration of Collision ‘Consequence’ in Satellite Conjunction Assessment and Risk Analysis.” 26th International Symposium on Space Flight Dynamics, Matsuyama, Japan, June 2017.

49. Hejduk, M.D., D. E. Snow, and L. K. Newman. 2019. “Satellite Conjunction Assessment Risk Analysis for ‘Dilution Region’ Events: Issues and Operational Approaches.” Fifth Annual Space Traffic Management Conference Progress through Collaboration, Austin TX, February 2019.

50. Hejduk, M.D. and D. E. Snow. 2019. “Satellite Conjunction ‘Probability,’ ‘Possibility,’ and ‘Plausibility’: A Categorization of Competing Conjunction Assessment Risk Analysis Paradigms.” 2019 AAS/AIAA Astrodynamics Specialist Conference (Paper #19-652), Portland ME, August 2019.

51. Hoots, F. R. and R. L. Roehrich. 1980. “Spacetrack Report No.3 – Models for Propagation of NORAD Element Sets,” December 1980.

52. Jenkin, A.B., J. P. McVey, and G. E. Peterson. 2020. “Solution of long-coast re-entry COLA problems with COLA gap methods” Journal of Space Safety Engineering Volume 7, Issue 2, June 2020, Pages 105-112.

53. Johnson, N.L., P. H. Krisko, J. C. Liou, and P. D. Anz-Meador. 2001. “NASA’s New Breakup Model of EVOLVE 4.0.” *Advances in Space Research*, Vol. 28 No. 9 (2001), pp. 1377-1384.

54. Kaplan, S. and B. Garrick. 1981. “On the Quantitative Definition of Risk.” *Risk Analysis*, Vol. 1 No. 1 (1981), pp. 11-27.

55. Kessler, D. J. 1981. “Derivation of the Collision Probability between Orbiting Objects: The Liftetimes of Jupiter’s Outer Moons,” *Icarus*, Vol. 48 (1981), pp. 39-48.

56. Lebedev, V., and Laikov, D. 1999. “A Quadrature Formula for the Sphere of the 131st Algebraic Order of Accuracy,” *Doklady Mathematics*, Vol. 59, No. 3 (1999), pp. 477-481.

57. Lechtenberg, T. F. and M. D. Hejduk. 2019. “Assessment and Validation of Collision ‘Consequence’ Method of Assessing Orbital Regime Risk Posed by Potential Satellite Conjunctions.” 2019 Hypervelocity Impact Symposium, Destin FL, March 2019, HVIS2019-061.

58. Lechtenberg, T. 2019a. “An Operational Algorithm for evaluating Satellite Collision Consequence.” 2019 AAS Astrodynamics Specialist Conference (Paper #19-669), Portland ME, August 2019.

59. Lechtenberg, T., 2019b. “Multivariate Normality of Cartesian-Framed Covariances: Evaluation and Operational Significance.” 2019 AAS Astrodynamics Specialist Conference (Paper #19-671), Portland ME, August 2019.

60. Li, Z., Ziebart, M., Bhattarai, S., Harrison, D., Grey, S. 2018. “Fast Solar Radiation Pressure Modelling with Ray Tracing and Multiple Reflections.” Advances in Space Research, Vol. 61, No. 9, pp. 2352-2365.

61. Mashiku, A.K. and M. D. Hejduk. 2019. “Recommended Methods for Setting Mission Conjunction Analysis Hard Body Radii.” 2019 AAS Astrodynamics Specialist Conference (Paper #19-702), Portland ME, August 2019.

62. Mclean, F., Lemmens, S., Funke, Q., Braun, V. 2017. “DISCOS 3: An Improved Model for ESA’s Database and Information System Characterising Objects in Space.” Proc. 7th European Conference on Space Debris, Darmstadt, Germany, June 2017.

63. Patera, R.P. 2001. “General Method for Calculation Satellite Collision Probability. 2001. ” Journal of Guidance, Control, and Dynamics, Vol. 24, No. 4 (July-August 2001), pp. 716-722.

64. Press, W. H., Teukolsky, S. A., Vettering, W. T., and Flannery, B. B. 1992. *Numerical Recipes in FORTRAN: The Art of Scientific Computing*, 2nd ed., Cambridge University Press, New York, NY, 1992.

65. Rosenberg, F. 2003. “Radar Characterization of RORSAT Coolant Spheres and their Potential Use for Calibration and Validation of Debris Tracking Sensors.” MIT Lincoln Laboratory Project Report STK-264, November 2003.

66. Rosner, B. 1975. “On the Detection of Many Outliers.” *Technometrics* 17 (1975), 221-227.

67. Rosner, B. 1977. “Percentage Points for the RST Many Outlier Procedure.” *Technometrics* 19 (1977), 307-312.

68. Sabol, C., T. Sukut, K. Hill, K. Alfriend, B. Wright, Y. Li, and P. Schumacher. 2010. "Linearized orbit covariance generation and propagation analysis via simple Monte Carlo simulations." AAS/AIAA Space Flight Mechanics Meeting (paper AAS-10-134), San Diego, CA, February 2010.

69. Schilling, B., Y. Taleb,, J. Carpenter, M. Balducci, and T. Williams. 2016. "Operational Experience with the Wald Sequential Probability Ratio Test for Conjunction Assessment from the Magnetospheric MultiScale Mission." 2016 AIAA/AAS Astrodynamics Specialist Conference, Long Beach CA, August 2016.

70. Seitzer, P. 2020. (U MI) "Large Constellations of LEO Satellites and Astronomy." Advanced Maui Optical and Space (AMOS) Surveillance Technologies Conference, September 15-18, 2020.

71. Shelton, C.T. and J. L. Junkins. 2019. "Probability of Collision between Space Objects Including Model Uncertainty." *Acta Astronautica*, Vol.155 (2019), pp.462-471.

72. Sivia, D.S. and Skilling, J. 2006. *Data Analysis: A Bayesian Tutorial.* 2nd ed., Oxford, UK, Oxford University Press.

73. Stokely, C.L., Foster, J.L., Stanbery, E.G., Benbrook, J.R., and Juarez, Q. 2006. "Haystack and HAX Radar Measurements of the Orbital Debris Environment." National Aeronautics and Space Administration Report, Orbital Debris Program Office, (JSC-62815), Nov. 2006.

74. Tarzi, Zahi B., Brian T. Young, David S. Berry. 2022. "Deriving Event Thresholds and Collision Probability for Automated Conjunction Assessment at Mars and the Moon", AAS 22-042, 2022 American Astronomical Association (AAS)/American Institute of Aeronautics and Astronautics (AIAA) Astrodynamics Specialist Conference, Charlotte, NC, August, 2022. https://www.nasa.gov/cara/madcap.

75. Tobiska, W.K., D. Knipp, W. J. Burke, D. Bouwer, J. Bailey, D. Odstrcil, M. P. Hagan, J. Gannon, and B. R. Bowman. 2013. "The Anemomilos Prediction Methodology for Dst." *Space Weather* (Vol. 11, No. 9 (September 2013) pp 490-508. DOI: 10.1002/swe.20094.

76. Walker, C. et al. 2020, "Impact of Satellite Constellations on Optical Astronomy and Recommendations Toward Mitigations." *SatCon-1 Workshop Report*, NSF NOIRLab, Aug 2020.

77. Walker, C. et al. 2021. "Executive Summary." *Report of the SatCon-2 WorkShop*, NSF NOIRLab, Jul 2021.

78. Vallado 1981.

79. Vallado, D.A. 2001. *Fundamentals of Astrodynamics and Applications.* 2nd ed. El Segundo, CA, Microcosm Press.

80. Woodburn, J. and S. Tanygin. 2014. "Coordinate Effects on the use of Orbit Error Uncertainty." International Symposium on Space Flight Dynamics 24 (Baltimore, MD), May 2014.

National Aeronautics and Space Administration

Headquarters